Prohibitin depletion extends lifespan of a TORC2/SGK-1 mutant through autophagy

Blanca Hernando-Rodríguez[1,2,*], Mercedes M. Pérez-Jiménez[1,2,*], María Jesús Rodríguez-Palero[1,2], Antoni Pla[1,2], Manuel David Martínez-Bueno[1,2], Patricia de la Cruz Ruiz[1,2], Roxani Gatsi[1,2] and Marta Artal-Sanz[1,2 #]

[1]Andalusian Centre for Developmental Biology, Consejo Superior de Investigaciones Científicas/Junta de Andalucía/Universidad Pablo de Olavide, Seville, Spain

[2]Department of Molecular Biology and Biochemical Engineering, Universidad Pablo de Olavide, Seville, Spain

[#]Correspondence to: martsan@upo.es

*Equal contribution

Mitochondrial prohibitins (PHB) are highly conserved proteins with a peculiar effect on lifespan. While PHB depletion shortens lifespan of wild type animals, it enhances longevity of a plethora of metabolically compromised mutants, including target of rapamycin complex 2 (TORC2) mutants *sgk-1* and *rict-1*. Here, we show that *sgk-1* mutants have impaired mitochondrial homeostasis, lipogenesis, yolk formation and autophagy flux due to alterations in membrane lipid and sterol homeostasis. Remarkably, all these features are suppressed by PHB depletion. Lifespan analysis shows that autophagy and the mitochondrial unfolded protein response (UPR^{mt}), but not mitophagy, are required for the enhanced longevity caused by PHB depletion in *sgk-1* mutants. We hypothesize that UPR^{mt} induction upon PHB depletion extends lifespan of *sgk-1* mutants through autophagy. Our results strongly suggest that PHB depletion suppresses the autophagy defects of *sgk-1* mutants by altering membrane lipid composition at ER-mitochondria contact sites, where TORC2 localizes.

30 ## Introduction

31 Mitochondrial function, nutrient signalling and autophagy regulate aging across phyla.
32 However, their exact mechanisms and interactions in lifespan modulation still remain
33 elusive. The mitochondrial prohibitin (PHB) complex is a strongly evolutionarily
34 conserved ring-like macromolecular structure (Artal-Sanz and Tavernarakis, 2009a;
35 Merkwirth and Langer, 2009). While deletion of PHB does not cause any observable
36 growth phenotype in the unicellular yeast *Saccharomyces cerevisiae* (Osman et al.,
37 2009), in *Caenorhabditis elegans* the PHB complex is required for embryonic
38 development and its postembryonic depletion leads to morphological abnormalities in
39 the somatic gonad and sterility (Artal-Sanz et al., 2003). Prohibitins have been implicated
40 in several age-related diseases (Nijtmans et al., 2002; Thuaud et al., 2013) and are
41 involved in mitochondrial morphogenesis and membrane maintenance by acting as
42 chaperones (Nijtmans et al., 2000) and scaffolds (Merkwirth et al., 2012). PHB depletion
43 has been shown to perturb mitochondrial homeostasis causing an induction of the
44 mitochondrial unfolded protein response, UPR^{mt} (Benedetti et al., 2006; Hernando-
45 Rodriguez et al., 2018; Yoneda et al., 2004).

46 PHB depletion has opposing effects on lifespan depending on the genetic background.
47 Loss of PHB by RNAi shortens lifespan in wild type worms, whereas it increases lifespan
48 in different metabolically compromised backgrounds. These include mutants of the
49 Insulin/IGF-1 signalling (IIS) pathway and mutants with compromised mitochondrial
50 function or fat metabolism (Artal-Sanz and Tavernarakis, 2009b). In particular, PHB
51 depletion increases lifespan of the long-lived *daf-2(e1370)* mutants, where the induction
52 of the UPR^{mt} is reduced (Gatsi et al., 2014). Analysis of known kinases acting
53 downstream of the insulin receptor DAF-2 revealed that loss of function of SGK-1 in PHB
54 depleted animals results in enhanced longevity and reduced UPR^{mt} activation similar to

55 that observed in PHB depleted *daf-2* mutants (Gatsi et al., 2014). SGK-1 belongs to the
56 AGC kinase family and is the sole *C. elegans* homologue of the mammalian Serum- and
57 Glucocorticoid-inducible Kinase. Its activation depends on PI3K and has been involved
58 in response to oxidative stress and DNA damage, among others (Di Cristofano, 2017).
59 In addition to acting in the IIS pathway, SGK-1 regulates aging and mitochondrial
60 homeostasis through a parallel pathway, as part of TORC2 (Target Of Rapamycin
61 Complex 2), downstream of RICT-1. Interestingly, depletion of PHB in *daf-2;sgk-1* double
62 mutants enhances both the increased lifespan and the reduction of the UPR^{mt} (Gatsi et
63 al., 2014).

64 Work in yeast has demonstrated that Ypk1, the yeast homologue of SGK-1, is the
65 relevant target of TORC2. Ypk1 is involved in sphingolipid synthesis and ceramide
66 signalling, having an essential role in lipid membrane homeostasis and affecting cell size
67 and growth rate (Lucena et al., 2018; Muir et al., 2014; Roelants et al., 2018). TORC2-
68 Ypk1 controls sphingolipid homeostasis by sensing and regulating ROS (Niles et al.,
69 2014). Moreover, TORC2-Ypk1 regulates autophagy induced by amino acid starvation
70 (Vlahakis et al., 2014) and modulates the autophagy flux by controlling mitochondrial
71 respiration and calcium signalling (Vlahakis et al., 2016; Vlahakis et al., 2017). The
72 underlying molecular mechanism remains however unknown. In worms, SGK-1
73 regulates development, fat metabolism, stress responses and lifespan in a complex and
74 controversial manner, partially explained by the different alleles under study and the
75 different growing conditions (Chen et al., 2013; Dowen et al., 2016; Gatsi et al., 2014;
76 Hertweck et al., 2004; Jones et al., 2009; Mizunuma et al., 2014; Soukas et al., 2009;
77 Tullet et al., 2008; Zhou et al., 2019).

78 To better understand how SGK-1 regulates lifespan and mitochondrial function, we
79 explored the interaction between PHB and SGK-1. Our results show that long-lived *sgk-*
80 *1(ok538)* mutants have altered mitochondrial structure and function, phenotypes that are

81 suppressed by PHB depletion. A transcription factor RNAi screen identified membrane
82 lipid homeostasis as a mechanism implicated in SGK-1 mediated maintenance of
83 mitochondrial function. In agreement with that, electron microscopy analysis showed
84 defects in organelle membrane contact sites in *sgk-1* mutants, leading to defective
85 lipogenesis and lipoprotein production and a blockage of the autophagic flux.
86 Remarkably, these phenotypes are suppressed by PHB depletion. Furthermore, lifespan
87 analyses showed that autophagy and the UPR^{mt} are required for the enhanced longevity
88 of *sgk-1* mutants upon PHB depletion, while mitophagy is not. Consequently, in the
89 absence of the PHB complex, SGK-1 expression levels increased upon inhibition of the
90 UPR^{mt}, but are not affected by inhibition of mitophagy. Our data strongly suggest that
91 UPR^{mt} induction upon PHB depletion extends lifespan of *sgk-1* mutants through
92 autophagy. We discuss our observations in light of the conserved role of TORC2 in lipid
93 membrane biology and the proposed role of the PHB complex and TORC2 at
94 mitochondria-associated endoplasmic reticulum (ER) membranes (MAM).

95

96 ## Results

97 **Prohibitin depletion suppresses the altered mitochondrial structure and**
98 **function of *sgk-1* mutants**

99 In *C. elegans*, loss of function of SGK-1 causes a delay in development (Jones et al.,
100 2009) as well as reduced brood and body size (Soukas et al., 2009). These phenotypes
101 are consistent with phenotypes observed in mitochondrial mutants (Dillin et al., 2002). In
102 addition, worms lacking the TORC2 component RICT-1 or the downstream kinase SGK-
103 1, have an induced mitochondrial unfolded protein response (UPR^{mt}) (Gatsi et al., 2014).
104 We analyzed whether mitophagy, another mitochondrial quality control mechanism,
105 might be activated in *sgk-1* deletion mutants using a mitophagy reporter based on PINK-
106 1 protein (Kirienko et al., 2015). PINK-1 is a serine threonine protein kinase that, when
107 mitochondria are depolarized, accumulates in the outer mitochondrial membrane and
108 targets mitochondria for selective autophagy (Narendra and Youle, 2011; Palikaras et
109 al., 2015). We observed that depletion of *sgk-1* increased PINK-1 protein levels (Figure
110 1A). Similarly, PINK-1 protein levels increased upon depletion of *phb-1* or *atfs-1,* the key
111 UPR^{mt} regulator (Figure 1A), confirming that *sgk*-1 mutants suffer from mitochondrial
112 stress.

113 To better define the mitochondrial defect of *sgk-1* deletion mutants we performed
114 transmission electron microscopy (TEM) analysis. Mitochondria in *sgk-1* mutants were
115 swollen, and bigger compared to wild type worms in all tissues analyzed (hypodermis,
116 muscle and intestine) at both, day one and day five of adulthood (Figure 1B and Figure
117 S1A, respectively). In contrast to previous observations (Zhou et al., 2019), no obvious
118 mitochondrial fragmentation or severe cristae defects in the intestine were observed in
119 the TEM sections analyzed.

120 To better understand the interaction between PHB and SGK-1, we measured
121 mitochondrial performance in *sgk-1* mutants in the presence or absence of the PHB
122 complex, during aging (Figures 1C-F and Figure S1B-C). At the young adult stage, *sgk-*
123 *1* mutants showed a dramatic increase in basal OCR compared to wild type worms
124 (Figures 1C and 1D), consistent with the previous finding that mammalian
125 mTORC2/rictor knockdown leads to an increase in mitochondrial respiration in
126 mammalian cells (Schieke et al., 2006). The increased respiration rate of *sgk-1* mutants
127 is suppressed by PHB depletion, which also reduces the OCR of wild type young adult
128 worms (Figures 1C and 1D). At day 6 of adulthood, the OCR was reduced compared to
129 young animals (Figure S1C) as described (Van Raamsdonk et al., 2010), but not in *phb-*
130 *1(RNAi)* worms (Figure S1C). In *sgk-1* mutants, respiration dramatically drops during
131 aging, to the level of wild type animals. However, PHB depletion increases the OCR in
132 wild type and *sgk-1* mutants at day 6 of adulthood (Figure S1B and S1C). This suggests
133 that mitochondrial function declines with age in wild type animals but this decline occurs
134 at a higher rate in *sgk-1* mutants. In contrast, respiration remains relatively constant in
135 PHB depleted worms, where respiration is compromised already at the young adult
136 stage.

137 Measurements of maximal respiratory capacity at the young adult stage showed that
138 *sgk-1* mutants had a higher maximal respiratory capacity compared to wild type worms,
139 which was fully suppressed by PHB depletion. PHB depletion also reduced the maximal
140 respiratory capacity of wild type worms (Figure 1D). The spare capacity, is the difference
141 between maximal and basal OCR and it is defined as the amount of oxygen that is
142 available for cells under stress or increased energy demands. *sgk-1* mutants showed an
143 insignificant spare respiratory capacity compared to wild type animals. Additionally,
144 depletion of *phb-1* reduced the spare capacity of both *sgk-1* and wild type animals
145 (Figure 1D). We observed increased ATP-linked OCR in *sgk-1* mutants (Figure 1E),

146 which may correspond to a higher energy demand. *phb-1(RNAi)* reduced the ATP-linked
147 OCR (Figure 1E) both in otherwise wild type worms and in *sgk-1* mutants, suggesting
148 that the oxidative phosphorylation system was severely compromised. Again, depletion
149 of the PHB complex reversed *sgk-1* mutant phenotype, bringing ATP-linked OCR to wild-
150 type levels (Figure 1E). The O_2 consumed after sodium azide (NaN_3) injection
151 corresponds to the respiration caused by other cellular processes than oxidative
152 phosphorylation, such as non-mitochondrial NADPH oxidases or reactive oxygen
153 species production. Interestingly, *sgk-1* mutants showed an increased non-mitochondrial
154 respiration compared to wild type at the young adult stage, which was suppressed by
155 PHB depletion. Lack of PHB also reduced non-mitochondrial respiration in wild type
156 worms (Figure 1F).

157 Mitochondrial respiration is the predominant source of cellular ROS. We thus evaluated
158 ROS levels in *sgk-1* mutants in the presence and absence of the PHB complex. We
159 measured ROS formation in young adults using the dye H2-DCFDA (Figure 1G). In
160 agreement with the observed increase in both, mitochondrial and non-mitochondrial
161 respiration, *sgk-1* mutants showed dramatically elevated ROS levels in comparison to
162 wild type worms, as previously published in other organisms (Niles et al., 2014; Wang et
163 al., 2019). Depletion of *phb-1* increased ROS levels in wild type worms (Figure 1G and
164 (Artal-Sanz and Tavernarakis, 2009b)). However, depletion of *phb-1* reduced ROS levels
165 in *sgk-1* mutants (Figure 1G). Since H2-DCFDA measures mostly cytosolic ROS, these
166 results indicate that *sgk-1* mutants have high levels of cytosolic ROS that are reduced
167 upon *phb-1* depletion. Since increased mitochondrial ROS extends lifespan of
168 mitochondrial mutants with high levels of cytoplasmic ROS (Schaar et al., 2015), we
169 wondered whether the enhancement of lifespan upon *phb-1* depletion in *sgk-1* mutants
170 may be due to an increase in mitochondrial ROS levels. Absence of cytosolic superoxide
171 dismutase, *sod-1*, did not affect lifespan of wild type worms, while lack of the

172 mitochondrial superoxide dismutase, *sod-2*, increased wild type lifespan (Figure S1D,
173 Table S1 and (Van Raamsdonk and Hekimi, 2009; Yang and Hekimi, 2010)).
174 Interestingly, lack of *sod-1* reduced lifespan of *sgk-1* mutants, indicating that increased
175 cytosolic ROS is detrimental for *sgk-1* lifespan, while depletion of *sod-2*, increased
176 lifespan of *sgk-1* mutants (Figure S1E, Table S1), similar to mitochondrial mutants
177 (Schaar et al., 2015). In order to test if mitochondrial ROS generation upon PHB
178 depletion extends lifespan of *sgk-1* mutants, we treated animals with the antioxidant N-
179 acetyl-cysteine (NAC). NAC did not affect the lifespan of wild type worms or *sgk-1*
180 mutants. However, it shortened that of *phb-1* depleted backgrounds, both wild type and
181 *sgk-1* mutants (Figure S1F and S1G, Table S1). Therefore, we cannot conclude that
182 ROS is responsible for the lifespan extension conferred by PHB depletion to *sgk-1*
183 mutants.

184 Finally, we wondered whether depletion of the PHB complex would suppress the
185 increased mitochondrial size observed in *sgk-1* mutants. TEM analysis of muscle
186 mitochondria showed that *phb-1* depletion drastically reduced mitochondrial size in *sgk-*
187 *1* mutants, and resulted in mitochondrial fragmentation as it happens in otherwise wild
188 type worms (Artal-Sanz et al., 2003) (Figure 1H).

189 **Altered membrane sterol and lipid homeostasis induces the UPR^{mt} in the**
190 **TORC2/SGK-1 mutant.**

191 In order to understand the interaction of PHB with SGK-1 in lifespan regulation, we
192 looked for transcription factors mediating the UPR^{mt} in *sgk-1* mutants, as they might be
193 implicated in the activation of pro-survival pathways responsible for the long lifespan
194 observed in PHB-depleted TORC2 mutants (Gatsi et al., 2014). Several transcription
195 factors have been involved in the maintenance of mitochondrial homeostasis and
196 lifespan, including DAF-16, SKN-1, HIF-1 and HSF-1 (Fang et al., 2017; Hwang et al.,

197 2014; Kamal et al., 2016; Labbadia et al., 2017; Lee et al., 2010; Mouchiroud et al., 2013;
198 Palikaras et al., 2015; Senchuk et al., 2018; Tullet et al., 2008; Wu et al., 2018b).
199 Moreover, the UPR^{mt} promotes longevity by activating HIF-1, DAF-16 and SKN-1 (Wu et
200 al., 2018b). We investigated the involvement of these transcription factors in the
201 activation of the UPR^{mt} in *sgk-1* mutants and the essential TORC2 component *rict-1.*
202 Lack of DAF-16 slightly induced mitochondrial stress in wild type animals, while only HIF-
203 1 depletion futher induced the UPR^{mt} in *sgk-1* mutants (Figure 2A). However, in the *rict-*
204 *1* mutant, depletion of all the transcription factors enhanced the UPR^{mt} (Figure S2A).
205 This suggests that TORC2 deficiency modulates the UPR^{mt} through other kinases in
206 addition to *sgk-1*. Nevertheless, depletion of none of the transcription factors tested
207 inhibited the expression of *hsp-6*, suggesting that different mechanisms are implicated
208 in the UPR^{mt} in TORC2/SGK-1 mutants.

209 With the aim of understanding the mechanism by which SGK-1 might regulate
210 mitochondrial function, and possibly aging, we performed an RNAi screen. We knocked-
211 down 836 transcription factors of the *C. elegans* genome and quantified the expression
212 of the mitochondrial stress response reporter. We found 20 genes whose depletion
213 reduced the expression of P*hsp-6*::GFP in *sgk-1* mutants (FC $<$ 0.6) (Figure 2B). HIF-1
214 depletion did not increase P*hsp-6*::GFP (average FC 1.067) in our screen, while it did
215 when assayed on plate (Figure 2A). One possible explanation is that liquid growing
216 conditions are energetically more demanding, metabolism is altered and the UPR^{mt} might
217 be differentially regulated (Lev et al., 2019). We then looked for genetic interactors by
218 focusing on those transcription factors that when depleted reduced both the UPR^{mt} and
219 the size of *sgk-1* mutants (Figure 2C).

220 Interestingly, 2 of these candidates, *lin-40* and *ceh-20*, are involved in endocytic traffic
221 (Balklava et al., 2007). SGK-1 has been reported to be involved in endocytosis and
222 membrane trafficking in different models (Bomberger et al., 2014; Bourgoint et al., 2018;

223 deHart et al., 2002; Zhu et al., 2015) which supports the validity of the screen. We
224 identified several nuclear hormone receptors (NHRs), a family of ligand-regulated
225 transcription factors that are activated by steroid hormones, that play vital roles in the
226 regulation of metabolism, reproduction, and development. Among them is NHR-8, a
227 nuclear hormone receptor that regulates cholesterol levels, fatty acid desaturation and
228 apolipoprotein production (Magner et al., 2013). NHR-8 is required for dietary restriction-
229 mediated lifespan extension in *C. elegans* (Chamoli et al., 2014; Thondamal et al., 2014)
230 but also normal lifespan (Magner et al., 2013). Also related with cholesterol is SBP-1,
231 the homologue of sterol regulatory element binding protein SREBP-1. SREBPs are
232 required to produce cholesterol (Brown and Goldstein, 1997) and regulate the
233 expression of lipogenic genes across phyla (Horton et al., 2002; Walker et al., 2011).
234 Interestingly, mammalian mTORC2 activates lipogenesis through SREBP-1 in the liver
235 (Hagiwara et al., 2012). Similarly, in *C. elegans,* SBP-1 acts downstream of TOR and IIS
236 pathways and affects adult lifespan. Depletion of *sbp-1* does not affect lifespan of wild
237 type animals, but suppresses the increase in lifespan caused by pharmaceutical
238 inhibition of TGF-β and IIS signaling (Admasu et al., 2018).

239 In summary, we identified transcription factors involved in sterol metabolism, lipogenesis
240 and lipid membrane biology, whose depletion further reduced the size of *sgk-1* mutants
241 (Figure 2C), indicating a genetic interaction in *C. elegans*. Combining mutations in genes
242 that perturb the same process are expected to enhance the observed phenotypes. Loss
243 of function of SGK-1 reduces worm size, slows down development (Jones et al., 2009;
244 Soukas et al., 2009) and induces the UPR^{mt} (Gatsi et al., 2014). Depletion of both, NHR-
245 8 and SBP-1, exacerbated those phenotypes in *sgk-1* mutants at the young adult stage,
246 further reducing worm size and inducing the UPR^{mt} (Figure 2D). As reported, SBP-1
247 depletion reduced the size of wild type animals (Nomura et al., 2010) as did depletion of
248 NHR-8. However, while depletion of neither NHR-8 nor SBP-1 affected development of

249 wild type animals, it specifically slowed down the developmental rate of *sgk-1* mutants
250 (Figure S2B), indicating a synthetic interaction. Moreover, depletion of both, NHR-8 and
251 SBP-1, mimicked the induced UPR^{mt} observed in *sgk-1* loss-of-function mutants (Figure
252 2D). Apart from sterol (Roelants et al., 2018), ceramide and sphingolipids are also key
253 structural lipids of membranes that are regulated by Ypk1/SGK-1 in yeast (Berchtold et
254 al., 2012; Muir et al., 2014; Niles et al., 2014; Roelants et al., 2011) and regulate
255 membrane trafficking in *C. elegans* (Zhang et al., 2011). We targeted by RNAi *sptl-1,* a
256 serine palmitoyl-CoA acyltransferase responsible for the first committed step in *de novo*
257 sphingolipid synthesis, and *cgt-3,* a ceramide glucosyltransferase, previously shown to
258 interact with SGK-1 (Zhu et al., 2015). Similar to NHR-8 and SBP-1, depletion of SPTL-
259 1 and CGT-3 induced the UPR^{mt} in otherwise wild type worms, similar to the *sgk1* mutant
260 phenotype (Figure S2C). As reported, *cgt-3* depletion caused a very slow developmental
261 phenotype in *sgk-1* mutants (Zhu et al., 2015). In addition, only 10-20% of animals
262 reached adulthood, while the rest arrested development as L3 larvae. Depletion of *sptl-*
263 *1* slightly slowed development and caused a partial (10 to 15%) larval arrest in otherwise
264 wild type animals, while 100% of *sgk-1* mutants arrested development at the L3 stage.
265 Thus, inhibition of ceramide and sphingolipids synthesis results in a synthetic interaction
266 with *sgk-1* mutants (Figure S2D). As they are not at the same developmental stage, *hsp-*
267 *6* expression levels cannot be compared, however, depletion of *sptl-1* and *cgt-3* seemed
268 to further induce the UPR^{mt} in *sgk-1* mutants (Figure S2D). These results together, show
269 that defective lipogenesis and/or altered cholesterol and sphingolipid metabolism cause
270 mitochondrial proteotoxic stress. Furthermore, the results indicate that the UPR^{mt}
271 observed in *sgk-1* mutants may be the result of altered lipid and sterol homeostasis.

272 **Prohibitin depletion suppresses lipogenesis and lipoprotein/yolk formation**
273 **defects in *sgk-1*.**

274 SREBPs are master regulators of lipogenesis and undergo sterol-regulated export from
275 the ER to the Golgi (Goldstein et al., 2006; Marks and Wood, 1992) where proteases
276 release the transcriptionally active protein (Brown and Goldstein, 1997). Also, transport
277 of ceramide from the ER to the Golgi is a crucial step in sphingolipid biosynthesis (Perry
278 and Ridgway, 2005). Both, in *C. elegans* and mammalian models, SREBPs are regulated
279 in response to altered membrane lipid ratios through ARF1 and GBF1 (Smulan et al.,
280 2016), which function in vesicular trafficking, lipid homoeostasis and organelle dynamics
281 (Kaczmarek et al., 2017). In *C. elegans* GBF-1 localizes in close proximity to the Golgi
282 and the ER-exit sites and is required for secretion and integrity of both organelles
283 (Ackema et al., 2013). GFB-1 and SGK-1 physically associate, GBF-1 being required for
284 proper localization of SGK-1 near the basolateral membrane of intestinal cells (Zhu et
285 al., 2015). Interestingly, ARF1 and GBF1 play an evolutionarily conserved role in ER-
286 mitochondria contact site functionality and lack of GBF-1 causes a similar increase in
287 mitochondrial size as *sgk-1* deletion in *C. elegans* ((Ackema et al., 2014) and Figure 1B
288 and S1).

289 Thus, we used transmitted electron microscopy (TEM) to explore whether TORC2/SGK-
290 1 plays a role in ER contacts and ER-mitochondria contact sites. We analyzed *sgk-1*
291 mutants at the beginning of the reproductive period (day 1 of adulthood) and at day 5 of
292 adulthood. We observed protruding structures from the endoplasmic reticulum,
293 resembling exit sites, which were not observed in wild type animals, where the ER
294 appeared compacted (Figure 3A, highlighted in Figure S3A and S3B). Lipid droplets
295 emanate from the ER (Salo and Ikonen, 2019) and both production and secretion of
296 lipoproteins are regulated via the ER-to-Golgi intermediary compartment (ERGIC)

297 (Brodsky and Fisher, 2008). Protruding ER exit sites (ERES) could reflect defective lipid
298 droplet formation and/or defective ER to Golgi or Golgi to ER secretion. TEM images
299 showed increased number of Golgi vesicles and increased size of the Golgi system in
300 *sgk-1* mutants (Figure 3A, highlighted in Figure S3A and S3B). The increased presence
301 of ERES indicates impaired lipid droplet and lipoprotein biogenesis, as evidenced by the
302 reduced content of lipid and yolk observed in *sgk-1* mutants (Figure 3A)(also visible in
303 Figure S1A). This agrees with the role of SGK-1 in lipogenesis and vitellogenesis in *C.*
304 *elegans* (Dowen et al., 2016; Wang et al., 2016; Yen et al., 2010). Interaction of lipid
305 droplets with yolk forming particles and vacuoles also appeared altered at day 1 of
306 adulthood and abnormal myelinated structures were visible (Figure S3B). At day 5, the
307 number of ERES was reduced as compared to day 1 in *sgk-1* mutants, instead, small
308 ER-emanating lipid droplets and myelinated structures/defective autolysosomes
309 accumulate (Figure 3A)(also visible in Figure S1A). These phenotypes could reflect
310 defective endomembrane biology in *sgk-1* mutants, in agreement with the proposed role
311 for *sgk-1* in membrane trafficking in *C. elegans* (Zhu et al., 2015) and yeast (Clarke et
312 al., 2017; deHart et al., 2002). In addition, the accumulation of ERES affects the proximity
313 of ER membranes to mitochondria. In wild type animals, the ER appeared compacted
314 and close to mitochondria, while in *sgk-1* mutants less contact between ER and
315 mitochondria was observed in the intestine and in muscle (Figure 3A and B,
316 respectively). This phenotype agrees with the observed localization of mTORC2 to
317 mitochondria-associated ER membranes (MAM) and defective MAM observed in liver-
318 specific mTORC2/rictor KO mice (Betz et al., 2013).

319 These results support a key role of SGK-1 in membrane trafficking, most likely by
320 affecting membrane lipid ratios and the formation of membrane contact sites, which
321 could explain all the observed phenotypes, i.e. defective mitochondrial function and
322 defects on lipid droplet and lipoprotein biogenesis. Since PHB depletion suppressed

323 mitochondrial defects of *sgk-1* mutants (Figure 1), we investigated if lack of the PHB
324 complex could suppress lipogenesis and yolk/lipoprotein accumulation. We analyzed
325 TEM sections at the beginning of the intestine, before and after the gonad turn, in 5 days
326 old animals (Figure 3C). *sgk-1* mutants were defective in lipid droplet formation and
327 vitellogenesis, as previously reported (Dowen et al., 2016; Yen et al., 2010). In addition,
328 little accumulation of lipoprotein pools at the pseudocoelom was observed compared to
329 wild type and PHB depleted animals (Figure 3C). Strikingly, depletion of the
330 mitochondrial PHB complex suppressed both, lipid droplet accumulation and yolk
331 production defects of *sgk-1* mutants (Figure 3C). Furthermore, *sgk-1* mutants showed all
332 the above described phenotypes when fed on OP50, a different bacterial food source
333 (Figure S3C). The phenotypes observed in OP50 bacteria-fed *sgk-1* mutants included
334 abnormal foci of myelinated forms, defective lipid droplet formation and generally
335 reduced lipid content and yolk, as well as increased mitochondrial size.

336 Autophagosomes receive lipids from the ER, ERES, ERGIC, the Golgi apparatus, as
337 well as from mitochondria and ER-mitochondria contact sites (Wei et al., 2018).
338 Moreover, inhibition of late stages of autophagy has been shown to prevent the
339 conversion of intestinal lipids into yolk and the accumulation of lipoprotein pools at the
340 pseudocoelom (Ezcurra et al., 2018). Thus, our TEM analysis strongly suggests that *sgk-*
341 *1* mutants suffer from a blockage of the autophagy flux.

342 **Prohibitin depletion suppresses the impaired autophagy flux of *sgk-1***
343 **mutants.**

344 SGK-1 has been shown to modulate autophagy both via induction and blockage of
345 autophagy (Andres-Mateos et al., 2013; Singh et al., 2013; Vlahakis et al., 2014; Vlahakis
346 et al., 2016; Vlahakis et al., 2017; Zhou et al., 2019) and we observed an accumulation
347 of abnormal autophagosomes in *sgk-1* mutants (Figure 3A and Figure S3B). To better

348 understand the interaction of PHB and SGK-1, we analyzed the autophagic state in *sgk-*
349 *1* mutants in the presence and in the absence of the PHB complex.

350 To quantify autophagy we used a strain carrying the intestinal autophagy reporter P*nhx-*
351 *2*::mCherry::LGG-1 (Gosai et al., 2010) which shows a diffused cytoplasmic expression
352 pattern under basal conditions. However, induction of autophagy results in a punctated
353 expression pattern due to the recruitment of LGG-1 to the autophagosomes. We
354 classified the level of autophagy based on 5 different categories from very low (animals
355 with a completely diffused expression pattern) to very high (animals with big
356 aggregations of LGG-1 all along the intestine) (see Materials and Methods and Figure
357 S4A). We quantified autophagy immediately after the reproductive period (day 5), when
358 LGG-1 puncta are more obvious. *sgk-1* mutants showed an enhanced autophagy signal
359 compared to wild type animals (Figure 4A), as previously described in worms (Lehmann
360 et al., 2013; Zhou et al., 2019). While depletion of the PHB complex significantly
361 increased LGG-1 puncta in otherwise wild type worms, no additive effect was observed
362 in *sgk-1* mutants upon *phb-1* depletion (Figure 4A). We knocked down *unc-51,* an
363 essential gene for autophagosome formation, as a control to ensure the signal visualized
364 in the transgenic line corresponds to autophagy and not to mCherry aggregation. *unc-*
365 *51(RNAi)* reduced the autophagic signal under all tested conditions (Figure S4B).

366 To better analyze autophagy flux, we performed electron microscopy analysis at day 5
367 of adulthood at the beginning of the intestine (see materials and methods). Characteristic
368 structures of impaired autophagy flux observed in TEM images of *C. elegans* are
369 abnormal foci with myelinated membranes (Toth et al., 2008). Myelinated forms including
370 multivesicular bodies, multilaminar bodies and myelinated membrane whorls were
371 clearly visible in *sgk-1(ok538)* mutants (Figure 4B). Quantification in the different
372 backgrounds (Figure 4B, bottom panel) showed that myelinated forms rarely appeared
373 in wild type and in *phb-1(RNAi)* treated worms, while they accumulated in *sgk-1* mutants.

374 Interestingly, the accumulation of myelinated forms in *sgk-1* mutants was suppressed
375 upon *phb-1(RNAi)* (Figure 4B). Altogether, the differences in LGG-1 expression pattern
376 and the accumulation of electro-dense particles, suggest that while autophagy is induced
377 in PHB depleted worms, both, induction of autophagy and an impairment in the
378 autophagic flux occurs in *sgk-1* mutants, as previously proposed in yeast (Vlahakis et
379 al., 2014; Vlahakis et al., 2016; Vlahakis et al., 2017).

380 We confirmed activation of autophagy in *sgk-1(ok538)* mutants by looking at the
381 subcellular localization of the transcription factor HLH-30/TFEB, a positive regulator of
382 autophagy, lysosome biogenesis and longevity (Lapierre et al., 2013; Settembre et al.,
383 2011). We observed increased nuclear localization of HLH-30 in *sgk-1* mutants (Figure
384 4C). In order to confirm blockage of autophagy in *sgk-1* mutants we pharmacologically
385 suppressed autophagy adding Bafilomycin A1 (BafA), an inhibitor of vacuolar type H^+-
386 ATPases that prevents lysosomal acidification causing a blockage of the autophagic flux
387 (Zhang et al., 2015). Upon bafilomycin treatment, wild type worms showed an increase
388 in LGG-1 aggregates (34%), which corresponds to the accumulation of non-degraded
389 autophagosomes (Figure 4D). Although Bafilomycin further increased aggregates in *sgk-*
390 *1* mutants (Figure 4D), this increase was considerably lower than the one observed in
391 wild type worms (11% vs 34%), showing a partial blockage of the autophagic flux. To
392 further confirm this blockage in *sgk-1* mutants we used the dual-fluorescent protein
393 reporter mCherry::GFP::LGG-1, which allows monitoring of autophagosomes (APs),
394 double-membrane vesicles that engulf cytosolic cargo, and autolysosomes (ALs), where
395 degradation of cargo takes place after APs fuse with lysosomes (Chang et al., 2017;
396 Kimura et al., 2007) (Figure 4E). Under the acidic environment of ALs, GFP is quenched,
397 therefore, ALs appear as red punctae, while APs appear as yellow [green and red]
398 punctae. In wild type animals most red puncta appeared also green, while in *sgk-1*
399 mutants we found a large amount of only red and abnormal intestinal puncta (Figure 4E)

400 indicating an accumulation of ALs. The same was true for the hypodermis, where *sgk-1*
401 mutants presented more ALs than wild type worms (Figure S4C). Further demonstrating
402 a role of SGK-1 in maintaining the autophagic flux, we observed a completely diffused
403 expression pattern of intestinal mCherry::LGG-1 in worms overexpressing SGK-1 at day
404 5 of adulthood and suppression of the increased autophagosomes observed upon *phb-*
405 *1* depletion (Figure S4D). Because autophagy is required for the conversion of intestinal
406 lipids into yolk, the suppression of abnormal autophagic structures upon PHB depletion
407 agree with the suppression of both, lipid droplet and yolk accumulation defects of *sgk-1*
408 mutants upon PHB depletion.

409 **PHB depletion increases longevity in *sgk-1* mutants through modulation of**
410 **autophagy and the UPR^{mt}, but not mitophagy**

411 We have shown that long-lived *sgk-1(ok538)* mutants and PHB depleted animals have
412 induced mitochondrial quality control mechanisms such as mitophagy and the UPR^{mt}
413 (Figure 1). Similarly, autophagy is induced in both *sgk-1* mutants and PHB depleted
414 animals, however, the autophagy defects of *sgk-1* mutants are suppressed by PHB
415 depletion (Figure 4). Therefore, we investigated the requirement of autophagy as well as
416 both mitochondrial quality control mechanisms for the lifespan extension conferred by
417 prohibitin depletion to *sgk-1* mutants. Depletion of ATFS-1 did not affect lifespan of wild
418 type animals (Figure 5A and Table S1) (Tian et al., 2016). Surprisingly, even though
419 prohibitin depleted worms and *sgk-1(ok538)* have induced UPR^{mt}, inhibiting this process
420 did not shorten their lifespan (Figures 5A and 5B and Table S1). However, preventing
421 the UPR^{mt} suppressed the longevity of *sgk-1;phb-1(RNAi)* treated mutants down to wild
422 type levels (Figure 5B and Table S1). Similarly, inhibiting autophagy by *unc-51(RNAi)*
423 treatment did not affect lifespan of *phb-1* depleted worms nor of *sgk-1(ok538)* mutants
424 (Figures 5C, 5D and Table S1), while it shortened that of *sgk-1;phb-1(RNAi)* treated

425 animals (Figure 5D and table S1). Treatment with *unc-51(RNAi)* shortened the lifespan
426 of wild type worms (Figure 5C, Table S1 and (Schiavi et al., 2013)). Autophagy is divided
427 in four different steps (Melendez and Levine, 2009): initiation, nucleation, elongation and
428 final fusion with lysosomes for lysis of the cargo. Likewise inhibition of initiation (*unc-*
429 *51(RNAi)*), inhibition of nucleation (*bec-1(RNAi)*) and inhibition of elongation (*atg-*
430 *16(RNAi)*) shortened lifespan of the *sgk-1;phb-1(RNAi)* treated mutants (Figure S5A).
431 Therefore, we conclude that both mechanisms, autophagy and the UPR^{mt}, are required
432 for the enhanced longevity of *sgk-1(ok538)* mutants upon PHB depletion, most likely
433 because the UPR^{mt} transcription factor is a positive regulator of autophagy.

434 We then assessed the requirement of mitophagy for the increased longevity of *sgk-1*
435 mutants caused by the absence of the mitochondrial PHB complex. Inhibition of
436 mitophagy did not affect lifespan of wild type worms (Figure 5E, Table S1 and (Palikaras
437 et al., 2015)). Interestingly, preventing mitophagy showed a beneficial effect on lifespan
438 of PHB depleted worms and *sgk-1* mutants (Figure 5E, 5F and table S1). However, in
439 the case of *sgk-1;phb-1(RNAi)* treated worms inhibition of mitophagy either did not affect
440 or increased lifespan (Figure 5F and Table S1). We confirmed the beneficial effects of
441 preventing mitophagy in *sgk-1* and *phb-1* deficient backgrounds depleting DCT-1, a
442 mitophagy receptor acting downstream of PINK-1 (Palikaras et al., 2015). Lack of DCT-
443 1 increased the lifespan of PHB depleted worms and *sgk-1* mutants (Figure S5B-C and
444 Table S1) without affecting the lifespan of wild type worms (Figure S5B and Table S1),
445 thus recapitulating *pink-1(RNAi)* phenotypes. In the case of *sgk-1;phb-1(RNAi)* treated
446 mutants, *dct-1* depletion increased lifespan in one out of two replicates (Figure S5C and
447 Table S1). These results show that mitophagy can be beneficial for lifespan under certain
448 conditions, but detrimental in certain pre-conditioned mutants such as *sgk-1* and PHB
449 depleted worms. What determines mitophagy being beneficial or detrimental deserves
450 further investigation.

451 Altogether, our results show that autophagy and the UPR^{mt} are required for the lifespan
452 extension conferred by PHB depletion while *pink-1* mediated mitophagy is not. In
453 agreement, in PHB depleted animals, inhibition of the UPR^{mt} resulted in a remarkable
454 increase of intestinal SGK-1 protein levels during aging, while mitophagy inhibition did
455 not (Figure 5G). Similar results were obtained when we pharmacologically induced
456 mitochondrial stress with paraquat (PQ)(Figure S5D). The high SGK-1 levels observed
457 during aging upon UPR^{mt} inhibition in combination with mitochondrial stress, could be
458 related to the role of ATFS-1 in autophagy induction. Autophagy is one of the
459 compensatory pathways induced to protect cells from severe mitochondrial defects
460 (Ventura et al., 2006) and has been suggested as a cytoprotective mechanism implicated
461 in the lifespan extension of *sgk-1* mutants upon PHB depletion (Gatsi et al., 2014). Thus,
462 in the absence of ATFS-1, SGK-1 might become more important in keeping an efficient
463 autophagy flux, as previously proposed (Vlahakis et al., 2016; Vlahakis et al., 2017). This
464 hypothesis is supported by the observation that depleting genes involved in different
465 steps of autophagy, such as initiation (*unc-51(RNAi)*) or nucleation (*bec-1(RNAi)*),
466 increased SGK-1 protein levels (Figure S5E).

467 To better understand the differential requirement of both mitochondrial quality control
468 mechanisms, UPR^{mt} and mitophagy, for the lifespan extension of *sgk-1* mutants upon
469 PHB depletion, we examined their contribution to the observed pool of autophagosomes
470 in *sgk-1* mutants, PHB depleted animals, and *sgk-1;phb-1(RNAi)* treated mutants (Figure
471 5H). When treating worms with *atfs-1(RNAi)* we observed a reduction in the autophagic
472 signal under all tested conditions (Figure 5H), as expected since ATFS-1 regulates
473 directly the expression of LGG-1 (Nargund et al., 2015). Treatment with *pink-1(RNAi)*
474 reduced the accumulation of autophagosomes in *phb-1(RNAi)* and in *sgk-1* mutants,
475 meaning that the signal observed in *phb-1(RNAi)* and in *sgk-1* mutants corresponds
476 partially to mitophagy (Figure 5G), which agrees with the observed increase in PINK-1

477 protein in *phb-1(RNAi)* and *sgk-1(RNAi)* treated worms (Figure 1A). However, inhibiting
478 mitophagy in *sgk-1;phb-1(RNAi)* did not significantly reduce the autophagosome pool
479 (Figure 5G). Therefore, it is tempting to speculate that the mechanism by which PHB
480 depletion extends *sgk-1* mutant lifespan is by inducing the UPR^{mt}, which in turn induces
481 general autophagy in a TORC2 independent manner.

482 Discussion

483 Depletion of PHB, a multimeric ring-like complex sitting in the inner mitochondrial
484 membrane induces the mitochondrial unfolded protein response (UPR^{mt}) and shortens
485 lifespan in wild type worms. In contrast, in a *sgk-1*-mutant background, PHB depletion
486 results in a further increase in lifespan and reduced activation of the UPR^{mt} (Gatsi et al.,
487 2014). In this work, we analyzed the interaction between the nutrient and growth factor
488 responsive kinase SGK-1 and the mitochondrial PHB complex. Our results strongly
489 suggest that mitochondrial, lipogenic and autophagic defects of *sgk-1* mutants are
490 caused by defective ER function and that PHB depletion suppresses those by altering
491 membrane lipid composition at ER-mitochondria contact sites, where TORC2 localizes,
492 having ultimately a beneficial outcome for lifespan.

493 mTORC2 and SGK-1 have previously been shown to regulate mitochondrial function by
494 maintaining mitochondria-associated ER membrane (MAM) integrity (Betz et al., 2013)
495 and SGK-1 has been reported to localize to mitochondria upon stress (O'Keeffe et al.,
496 2013). More recently, SGK-1 has been shown to phosphorylate VDAC1 at the outer
497 mitochondrial membrane, inducing its degradation (Zhou et al., 2019). The data we
498 present here supports a role for SGK-1 in MAM integrity. By electron microscopy we
499 described bigger mitochondria in *sgk-1* mutants compared to wild type (Figure 1B).
500 However, no obvious mitochondrial fragmentation or severe cristae defects could be
501 observed as previously described (Zhou et al., 2019). This might be due to different

502 growing conditions or the different alleles used. Although both predicted to be null alleles,
503 *ok538* is a deletion mutant (Hertweck et al., 2004), while *mg455* is a nonsense mutation
504 (Soukas et al., 2009). Nonsense mutations have been recently shown to trigger
505 compensatory mechanisms (Wilkinson, 2019). A more detailed analysis of the different
506 SGK-1 alleles is required to understand the different phenotypes observed. Similarly,
507 and contrary to what has been reported (Zhou et al., 2019), we described that *sgk-1*
508 mutants had a dramatic increase in oxygen consumption and a substantially reduced
509 reserve capacity (Figures 1C and 1D). A low reserve capacity corresponds to the
510 maximal usage of the mitochondrial capacity under normal conditions, which can be due
511 to mitochondrial defects that rescind the ability of the mitochondria to function at their full
512 potential, or to a continuous higher energy demand. Yeast Ypk1 deficient cells and *sgk-*
513 *1* mutant worms have reduced mitochondrial membrane potential (Aspernig et al., 2019;
514 Niles et al., 2014), which could indicate that a higher oxygen consumption is needed to
515 build up a membrane potential. Our observation agrees with the increased mitochondrial
516 respiration rate observed in mTORC2/rictor knockdown in mammalian cells (Schieke et
517 al., 2006). Consistent with increased respiration, *sgk-1* mutants had higher ROS levels
518 (Figure 1G and (Aspernig et al., 2019)). Interestingly, Ypk1 has been involved in both,
519 maintenance of, and response to, ROS levels (Niles et al., 2014). Although the molecular
520 bases of the connection between ROS levels and TORC2/Ypk1 signaling are unknown,
521 a link with sphingolipids homeostasis has been proposed (Niles et al., 2014). The authors
522 show that sphingolipids modulate suppression of ROS while sphingolipid depletion
523 activates Ypk1, via ROS signaling, that in turn functions as a positive regulator of
524 sphingolipid biosynthesis (Niles et al., 2014). Sphingolipids are essential components of
525 biological membranes, that together with ceramides regulate intracellular trafficking,
526 signaling and stress responses. TORC2/Ypk1 activates sphingolipid and ceramide
527 biosynthesis (Muir et al., 2014; Roelants et al., 2011). Furthermore, sphingolipids levels
528 modulate Ypk1 expression in a positive feedback loop to respond to membrane stress

529 (Berchtold et al., 2012) and to regulate cell growth (Lucena et al., 2018; Roelants et al.,
530 2018). In *C. elegans* SGK-1 has been proposed to regulate membrane trafficking through
531 sphingolipids (Zhu et al., 2015). We show here that depletion of *sptl-1* and *cgt-3*, key
532 genes in the synthesis of ceramides and sphingolipids, induced the UPR^{mt} as *sgk-1*
533 deletion mutants do (Figure S2C and (Gatsi et al., 2014)) and synthetically interact with
534 *sgk-1* (Figure S2B-D and (Zhu et al., 2015)). Interestingly, in worms, sphingolipid
535 biosynthesis has previously been linked to the UPR^{mt}, as phosphorylated sphingosine is
536 required in mitochondria to activate the UPR^{mt} (Kim and Sieburth, 2018). Inhibition of
537 sphingolipids biosynthesis reduces the induction of the UPR^{mt} due to a lack of ceramide,
538 which was demonstrated by the observation that ceramide supplementation rescues
539 *hsp-6* induction (Liu et al., 2014). Moreover, depletion of ceramide synthase genes and
540 sphingolipids synthesis increases lifespan (Cutler et al., 2014; Menuz et al., 2009;
541 Mosbech et al., 2013). These phenotypes resemble the effect of *sgk-1* deletion in PHB
542 depleted animals; reduced UPR^{mt} induction and increased lifespan (Gatsi et al., 2014).

543 Furthermore, our transcription factor RNAi screen uncovered the implication of
544 membrane sterol and lipid homeostasis in the UPR^{mt} induction triggered by SGK-1
545 deficiency (Figure 3B). Particularly interesting were NHR-8 and SBP-1/SREBP-1,
546 considering the role of Ypk1 in sphingolipid metabolism (Berchtold et al., 2012; Muir et
547 al., 2014; Niles et al., 2014; Roelants et al., 2011) and membrane sterol distribution at
548 plasma membrane-endoplasmic reticulum contact sites (Roelants et al., 2018). Here we
549 show that depletion of key transcription factors involved in lipogenesis and cholesterol
550 metabolism, NHR-8 and SBP-1 (Horton et al., 2002; Magner et al., 2013; Walker et al.,
551 2011), further enhances phenotypes associated with *sgk-1* mutants, including worm size
552 reduction, developmental delay, and induction of the UPR^{mt} (Figure 3D and S2).
553 Similarly, impaired vitellogenesis is also observed in both *nhr-8* and *sgk-1* mutants
554 (Dowen et al., 2016; Magner et al., 2013; Wang et al., 2016). These results show that

555 altered lipogenesis or membrane cholesterol signaling contribute to mitochondrial stress
556 and might be common processes regulated by SGK-1, NHR-8 and SBP-1. Mammalian
557 mTORC2 activates lipogenesis through SREBP-1 in the liver (Hagiwara et al., 2012).
558 Therefore, it is possible that deficiencies in building up cholesterol in *sgk-1* deficient
559 animals result in defective SREBP-1/SBP-1 activation. Moreover, cholesterol depletion
560 prevents SGK1 signaling in *Xenopus laevis* oocytes (Krueger et al., 2009) and, in yeast,
561 TORC2 signaling is regulated at membrane contact sites which facilitate the formation
562 of membrane domains composed of specialized lipids (Murley et al., 2017). Our data,
563 altogether, strongly suggest that, also in *C. elegans*, SGK-1 plays a key role in
564 membrane lipid composition and sterol homeostasis and that organellar membrane
565 contact sites could be modulated by TORC2/SGK-1 to coordinate cellular stress
566 responses.

567 Our TEM analysis showed that *sgk-1* mutants are defective in lipid droplet and
568 yolk/lipoprotein production, as well as pseudocelomic lipoprotein accumulation (Figure 4
569 and S3C). This is in concordance with the reduced lipid content and vitelogenesis
570 observed in *sgk-1* mutants (Dowen et al., 2016; Wang et al., 2016; Yen et al., 2010) and
571 with the proposed role of mTORC2, through SREBP1, in the regulation of lipogenesis by
572 (Hagiwara et al., 2012). Moreover, in various systems TORC2 has been linked to
573 functions in different membrane-contact sites (MCS) such as ER-plasma membrane
574 (Roelants et al., 2018) and ER-mitochondria (Betz et al., 2013). Our TEM analysis
575 supports a role for SGK-1 in ER homeostasis (Figure 4A and S3), in consonance with
576 the induced UPR^{ER} observed in *sgk-1(ok538)* mutants (Zhu et al., 2015) and the recent
577 uncovered role of SGK1 in the regulation of ER-dependent gene expression (Toska et
578 al., 2019). In addition, we observed that the ER was not as close to mitochondria as in
579 wild type animals, and in some areas in muscle cells no ER was observed at all (Figure
580 4B). In agreement with this, mammalian mTORC2 regulates mitochondrial physiology

581 (Schieke et al., 2006) by localizing to mitochondria-associated ER membrane (Betz et
582 al., 2013). Our study thus, indicates that SGK-1 plays a role in ER-mitochondria MCS
583 that is evolutionarily conserved. The ER consists of an elaborate network of membranes
584 that extends throughout the whole cell, making contacts with all organelles in the cell and
585 the plasma membrane (Wu et al., 2018a). Therefore, ER defects probably transcend to
586 all important roles of the ER in membrane biology, as we observed in *sgk-1* mutants.
587 These include defective lipid droplet formation and lipoprotein/yolk production.
588 Interestingly, we showed that mitochondrial PHB dysfunction suppresses defects in
589 lipogenesis and yolk/lipoprotein production (Figure 4C). Additionally, we observed
590 accumulation of myelinated structures/defective autolysosomes during aging in *sgk-1*
591 mutants (Figure 4A), which suggested a blockage of the autophagic flux, most likely due
592 to defective endomembrane interactions, as autophagosomes receive lipids from
593 essentially all organelles and organellar-contact sites (Wei et al., 2018). Importantly, we
594 identified a blockage of the autophagy flux in the last phase of autophagy, i.e.
595 degradation of the cargo (Figure 4E). This agrees with yeast data where Ypk1 mutants
596 show induced autophagy (Vlahakis et al., 2017) and reduced autophagy flux (Vlahakis
597 et al., 2016). Thus, blockage of autophagy is conserved in SGK-1 mutants. Interestingly,
598 depletion of PHB in *sgk-1* mutants reduced the accumulation of myelinated forms (Figure
599 4B). This is in line with findings in yeast, where autophagy flux is restored to wild-type
600 levels in *ypk1* deleted *rho0* cells or upon inhibition of mitochondrial respiration under
601 amino acid-starvation conditions (Vlahakis et al., 2016). This suggests that lack of PHB
602 can balance membrane lipid defects of *sgk-1* mutants.

603 We further demonstrate that the UPR^{mt} and general autophagy, but not mitophagy, play
604 an important role in PHB depleted *sgk-1* mutants. Autophagy and the UPR^{mt}, but not
605 mitophagy, are required for the lifespan extension conferred by PHB depletion to *sgk-1*
606 mutants (Figure 5, S5B-C and Table S1). Similarly, inhibition of the UPR^{mt}, but not

607 mitophagy, increase SGK-1 protein levels in PHB depleted animals (Figure 5G). And
608 finally, autophagy and the UPR^{mt}/ATFS-1, but not mitophagy, contribute to the pool of
609 autophagosomes in PHB-depleted *sgk-1* mutants (Figure 5H and S4B). We hypothesize
610 that inhibition of the UPR^{mt} mimics inhibition of autophagy because ATFS-1 is a positive
611 regulator of autophagy (Nargund et al., 2015). We speculate that the main function of
612 SGK-1 is to keep organelle membrane dynamics, therefore maintaining an efficient
613 autophagic flux. PHB depletion suppresses membrane defects of *sgk-1* mutants, making
614 autophagy and the UPR^{mt} beneficial and essential for lifespan. In line with this, SGK-1
615 protein levels increase in situations of strong mitochondrial stress (*phb-1* depletion or
616 PQ treatment) upon UPR^{mt} inhibition but not mitophagy inhibition (Figure 5G and S5D).
617 We hypothesize that in such conditions, inhibition of autophagy by inhibiting ATFS-1,
618 further increases the need of SGK-1 to keep an efficient autophagic flux. However, under
619 strong mitochondrial stress, inhibition of mitophagy does not affect SGK-1 levels
620 probably because mitophagy inhibition does not cause additional stress; instead it might
621 be beneficial to reduce mitochondrial clearance when mitochondria are severely
622 damaged and biogenesis is impaired. In fact, mitophagy is detrimental for both, PHB and
623 *sgk-1* single mutants (Figures 5E, 5F and Table S1), while autophagy and the UPR^{mt} are
624 not relevant (Figure 5B, 5D and Table S1). Recent data confirmed the beneficial effect
625 of inhibiting mitophagy for *sgk-1* development and reproduction (Aspernig et al., 2019).
626 Inhibition of autophagy results in increased SGK-1 protein levels (Figure S5E), further
627 supporting a role for SGK-1 in maintenance of the autophagic flux.

628 We show here that the PHB complex and SGK-1 interact functionally in maintaining
629 critical processes related to mitochondrial function, including ROS, lipid metabolism,
630 mitochondrial size and cytosolic ROS formation, lipogenesis, yolk production and
631 autophagy modulation. Elucidating the underlying molecular mechanisms behind the
632 observed functional interactions between the PHB complex and SGK deserves further

633 investigation. But many observations suggest that mitochondria associated ER
634 membranes, MAM, might be at play. MAM has been proposed as a hub for mTORC2-
635 Akt signaling (Betz and Hall, 2013) and TORC2/SGK1 plays a conserved role in
636 sphingolipid and ceramide biosynthesis (Berchtold et al., 2012; Lucena et al., 2018; Muir
637 et al., 2014; Roelants et al., 2011). The main function of MAM is to facilitate the transfer
638 of lipids and calcium between the two organelles (Csordas et al., 1999; Rizzuto et al.,
639 1998). MAM also mediates ER homeostasis and lipid biosynthesis by harboring
640 chaperones and several key lipid synthesis enzymes (Stone et al., 2009; Vance, 1990),
641 including synthesis and maturation of cholesterol, phospholipids and sphingolipids
642 (Fujimoto et al., 2012; Hamasaki et al., 2013; Raturi and Simmen, 2013; Verfaillie et al.,
643 2012). Besides, MAM of rat liver contains highly active sphingolipid-specific
644 glycosyltransferases (Ardail et al., 2003), and ceramide metabolism has been proposed
645 to occur at mitochondria as well as at MAM (Bionda et al., 2004). The PHB complex
646 affects membrane lipid composition and genetically interacts with proteins involved in
647 ER-mitochondria communication. PHB has been proposed to play a key role as
648 membrane organizer since it affects the distribution of cardiolipin and
649 phosphatidylethanolamine (Birner et al., 2003; Klecker et al., 2015; Osman et al., 2009).
650 In addition, lack of PHB in MEFs affects lipid metabolism and cholesterol biosynthesis
651 (Richter-Dennerlein et al., 2014). Moreover, PHB proteins have been genetically linked
652 to the mitochondrial inner membrane organizing system (MINOS) and to ER-
653 mitochondria encountered structures (ERMES) complexes in synthetic lethal screens in
654 yeast, forming part of a large ER-mitochondria organizing network, ERMIONE (Birner et
655 al., 2003; Kornmann et al., 2009; van der Laan et al., 2012). On the other hand, PHB
656 has been related with sphingosine metabolism as it interacts with sphigosine-1-
657 phosphate in mice mitochondria (Strub et al., 2011).

658 In the future, it will be important to decipher the role of SGK-1 at MAM and MCS at the

659 molecular level and the mechanism by which PHB depletion suppresses *sgk-1* defects.
660 We hypothesize an imbalance between PHB and SGK-1 activity caused by depletion of
661 either one has serious consequences for mitochondrial maintenance and cellular
662 homeostasis. Removing both restores balance. By studying the interaction of PHB with
663 TORC2/SGK-1 we unravel a conserved key role for both components in lipid
664 homeostasis. Our data demonstrates that PHB deficiency could alter membrane lipid
665 composition in a favorable manner for *sgk-1* mutants. Given the implication of TORC2,
666 PHB and autophagy in aging and cancer, our findings may contribute to ameliorate the
667 pathogenesis of aging-related disorders.

668

669 ## Materials and Methods

670 ### *C. elegans* strains and maintenance

671 The *C. elegans* strains used in this study were: N2 (wild type); MRS486: *sgk-1(ok538)X*
672 (3x outcrossed from BR4774, in total 11x outcrossed to N2 from the CGC strain VC345;
673 MRS88: *daf-2(e1370)III;* MRS68: *daf-2(e1370)III*;*sgk-1(ok538)X;* MRS386: *byEx*[*Psgk-*
674 *1::*SGK-1*::*GFP *+ rol-6(su1006)* (1x outcrossed from BR2773 (Hertweck et al., 2004))*;*
675 MRS38: *daf-2(e1370)III*;*byEx[*P*sgk-1::*SGK-1::GFP *+ rol-6(su1006)];* VK1093:
676 *vkEx1093[*P*nhx-2::*mCherry::LGG1]; MRS92: *sgk-1(ok538)X;vkEx1093[*P*nhx-*
677 *2::*mCherry::LGG1]; MRS112: *byEx[*P*sgk-1::*SGK-1::GFP *+ rol-6(su1006)];*
678 *vkEx1093[*P*nhx-2::*mCherry::LGG1]; SJ4100: *zcIs13[*P*hsp-6::*GFP*]V;* MRS19: *sgk-*
679 *1(ok538)X*;*zcIs13[*P*hsp-6::*GFP*]V;* MRS63: *rict-1(ft7)II*;*zcIs13[*P*hsp-6::*GFP*]V*; BR4006:
680 *pink-1(tm1779)II;byEx655[*P*pink-1::*PINK-1::GFP + P*myo-2::*mCherry + herring sperm
681 DNA]; MAH215: *sqIs11*[P*lgg-1*::mCherry::GFP::LGG-1 + *rol-6(su1006)*]; MRS555: *sgk-*
682 *1(ok538)X;sqIs11*[P*lgg-1*::mCherry::GFP::LGG-1 + *rol-6(su1006)*]; MAH240:

683 *sqIs17*[P*hlh-30*::HLH-30::GFP + *rol-6(su1006)*]; MRS558: *sgk-1(ok538)X;sqIs17*[P*hlh-*
684 *30*::HLH-30::GFP + *rol-6(su1006)*]; MRS505: *sod-1(tm776)II* (2x outcrossed to N2);
685 MRS516: *sod-1(tm776)II;sgk-1(ok538)X*; MRS504: *sod-2(gk257)I* (2x outcrossed to N2);
686 MRS510: *sod-2(gk257)I;sgk-1(ok538)X*.

687 Unless otherwise stated, we cultured the worms according to standard methods
688 (Brenner, 1974). We maintained nematodes at 20°C on nematode growth media (NGM)
689 agar plates seeded with live *Escherichia coli* OP50 (obtained from the CGC).

690 **RNAi assays on plates**

691 For RNAi experiments worms were placed on NGM plates, supplemented with 25 *µ*g/ml
692 carbenicillin (Sigma-Aldrich) and 10 *µ*g/ml nystatin (Sigma-Aldrich), seeded with HT115
693 (DE3) *Escherichia coli* bacteria (deficient for RNase-E) transformed with empty vector
694 (control) or the required target gene RNAi construct. Each bacterial strain was
695 inoculated, from an overnight pre-inoculum, in LB (ampicillin (100 *µ*g/ml) (Sigma-Aldrich)
696 and tetracycline (15 *µ*g/ml) (Sigma-Aldrich). The overnight culture was diluted (1:10) and
697 grown in a shaking incubator at 37°C for 3 hours, until it reached an OD_{600} of around 1.5.
698 Then, in order to induce the dsRNA expression, we added IPTG (final concentration: 1
699 mM) (Sigma-Aldrich) to the bacterial culture and we harvested the bacterial culture after
700 2 hours of incubation at 37°C by centrifugation (8 min at 6000×*g,* 4°C). Following, we
701 washed the pellets with S Basal and harvested them again. Finally, we re-suspended
702 bacterial pellets to a final concentration of 30 g/l in complete S Medium. Bacterial stocks
703 were kept at 4°C up to 4 days before being used. For all the RNAi treatments, bacterial
704 stocks were mixed in a proportion of 1:1 before seeding the plates.

705 A semi-synchronous embryo population was grown on plates seeded with the
706 appropriate RNAi bacterial clone at 20°C until the desired stage (young adult, day 1, day
707 5 or day 10 of adulthood). During the egg-laying period, we transferred worms every day

708 and every 2 days thereafter.

709 To pharmacologically induce a strong mitochondrial stress, we transferred L3 to fresh
710 RNAi plates containing 0.25 mM Paraquat (Sigma-Aldrich).

711 **Imaging**

712 On the day of imaging, worms were anesthetized with 10 mM Levamisole (Sigma-
713 Aldrich) or with a mixture of 10 mM Levamisole and 5 mM NaN_3 (Sigma-Aldrich) for
714 confocal imaging and mounted on 2% agarose pads. P*pink-1::*PINK-1::GFP, P*nhx-*
715 *2::*mCherry::LGG1 and P*sgk-1::*SGK-1::GFP reporter were observed using the AxioCam
716 MRm camera on a Zeiss ApoTome Microscope; P*lgg-1*::mCherry::GFP::LGG-1 reporter
717 was imaged with a confocal Nikon A1R equipped with a Plan Apo VC 60x/1.4 objective
718 and P*hsp-6::*GFP animals were visualized with a Leica M205 Stereoscope equipped with
719 a Plan Apo 5.0x/0.50 LWD objective and a ORCA-Flash4.0 LT Hamamatsu digital
720 camera.

721 Image analysis was performed using the ImageJ software. Emission intensity was
722 measured on greyscale images with a pixel depth of 16 bits. At least two independent
723 assays were carried out and the combined data was analyzed using the GraphPad Prism
724 software (version 5.0a).

725 **Electron microscopy**

726 Transmission electron microscopy (TEM) of *C. elegans* was carried out as described
727 (Hall et al., 2012) with small modifications. Adult worms, at day 1 or 5, were immersed
728 in 0.8% glutaraldehyde + 0.8% osmium tetroxide in 0.1 M sodium cacodylate buffer,
729 pH7.4. Carefully, under a dissecting scope, we cut the animals with a scalp at the
730 posterior end of the intestine, removing the tail, and kept the samples for 1 hour on ice
731 under dark conditions to allow complete penetration of the fixing solution. We washed

732 the worms three times with 0.1 M sodium cacodylate buffer and fixed them over night at
733 4°C in 2% osmium tetroxide in 0.1 M sodium cacodylate buffer; the entire procedure was
734 performed on ice. On the next day, we washed the worms three times with 0.1 M sodium
735 cacodylate buffer on ice and finally embedded the worms in small cubes of 1% agarose.
736 We then dehydrated the samples by incubating them in 50%, 70% and 90% ethanol for
737 10 minutes each, followed by 3 washes of 10 minutes each in 100% ethanol, at room
738 temperature. Next, we incubated the samples in a 50:50 ethanol/propylene oxide
739 solution for 15 minutes followed by 2 incubations of 15 minutes each in 100% propylene
740 oxide. We then infiltrated the samples on a rotator or with an embedding machine for 2
741 hours in a 3:1 ratio of propylene oxide to resin and next for 2 hours in a 1:3 ratio of
742 propylene oxide to 3 resin. Following, we incubated the samples overnight in 100% resin
743 and the next day changed to fresh 100% resin for 4 hours. We finally arranged the
744 samples in a flat embedding mold and cured them at 60°C for 2 days.

745 We cut the worms at the level of the first intestinal cells, immediately before and after the
746 gonad turn, specifically at 175 μm, 185 μm, 250 μm and 350 μm from the mouth.

747 For myelinated forms quantification, we analyzed 12 areas of 56 μm^2 per condition and
748 counted together multivesicular bodies (MVB), multillaminar bodies (MLB) and
749 myelinated forms. Data was analyzed using the GraphPad Prism software (version 5.0a).

750 **Oxygen consumption**

751 Worm oxygen consumption was measured using the Seahorse XFp Analyzer (Agilent)
752 as described (Luz et al., 2015). Briefly, worms at the young adults stage (30 per well)
753 or day 6 adult worms (20 per well), were transferred into M9-filled Seahorse plates.
754 OCR was measured 8 times in basal conditions as well as after each injection.
755 Working solutions were diluted in M9 at the final concentrations: FCCP (Sigma-
756 Aldrich) 250 µM, oligomycin (Sigma-Aldrich) 250 µM and NaN_3 (Sigma-Aldrich) 400

757 mM. Data were normalized by the protein content quantified by the bicinchoninic acid
758 assay (Thermofsiher). The OCR values were arranged in order to see the response
759 to the drug. Basal OCR corresponded to the average of the 8 measurements under
760 basal conditions, while the rest of the values derived from the average of the last 4
761 measurements. At least three independent assays were carried out and the combined
762 data was analyzed by *t*-test using GraphPad Prism software (version 5.0a).

763 **Quantification of Reactive oxygen species**

764 Cytoplasmic ROS was quantified using 2,7-dichlorofluorescin-diacetate (H2-DCFDA)
765 dye (Sigma-Aldrich) modified from (Artal-Sanz and Tavernarakis, 2009b). Briefly, 150
766 nematodes at the young adult stage were manually selected and recovered in M9 buffer
767 to a final concentration of 1 worm/μl. 50 μl of the worm suspension was transferred into
768 a 96-well flat bottom plate in triplicate (Thermo Fisher Scientific) and 50 μl of 100uM H2-
769 DCF-DA solution was added to the wells (H2-DCF-DA to a final concentration of 50 μM).
770 Immediately, basal fluorescence was measured (T_o) (Ex/Em: 485/520 nm) using a
771 microplate reader (PolarStar Omega. BMG, LabTech). After 1 hour of incubation at 20
772 ºC shaking, fluorescence was measure one again (T_1). The final fluorescence was
773 calculated by T_1-T_0. Data were normalized by the protein content quantified by the
774 bicinchoninic acid assay (BCA) (Thermo Fisher Scientific) and manually counting the
775 number of worms per well. At least three independent assays were carried out and the
776 combined data was analyzed by *t*-test using GraphPad Prism software (version 5.0a).

777 **Protein Content Quantification**

778 Total protein content was determined using the bicinchoninic acid (BCA) method.
779 Briefly, pellets from 50 worms were dried in a Speed Vac Concentrator (SPD12 1P
780 SpeedVac, Thermo Scientific), 20 *μ*l of 1 M NaOH were added to the dry pellet. Fat
781 was degraded by heating at 70°C for 25 min and 180 *μ*l of distilled water was added.

782 After vortexing, the tubes were centrifuged at 14000 rpm for 5 min and 25 μl of the
783 supernatant were transferred into a 96 well plate. Next, 200 μl of the BCA reagent,
784 prepared according to manufacturer's instructions (Pierce BCA Protein Assay Kit,
785 Thermo Scientific) was added to the sample. After incubation at 37°C for 30 min, the
786 plate was cooled to room temperature and absorbance was measured using the
787 POLARstar Omega luminometer (BGM Labtech) at 560 nm.

788 **Autophagy assays**

789 In order to monitor autophagy in *C. elegans* we used the reporter strain Ex[*Pnhx-*
790 *2*::mCherry::LGG-1] (Gosai et al., 2010). Animals were classified in 5 different
791 expression categories (Figure S4A): Very low: animals with a completely diffused
792 expression pattern; Low: animals with a generally diffuse expression pattern but with the
793 presence of small puncta; Medium: animals with puncta along the intestine; High:
794 animals showing aggregation of LGG-1 puncta mostly in the posterior part of the
795 intestine; Very high: animals with large LGG-1 aggregates along the whole intestine. To
796 avoid bias in the classification process, different researchers performed blind scoring on
797 the same animal images and disputes were resolved after discussion.

798 To determine whether increased levels of LGG-1 puncta corresponded to induced
799 autophagy or a blockage in the flux, we treated day 5 adult worms with Bafilomycine A_1
800 (BafA; Sigma-Aldrich), which blocks lysosome acidification. Animals were washed from
801 plates with M9 buffer and harvested in 15 ml tubes. In order to remove excess of bacteria,
802 we washed animals at least three times with M9 by letting the worms to settle at the
803 bottom of the tubes and then removed the supernatant. After washes, worms were
804 incubated for 6 hours in M9 with BafA (1.6 mM) or DMSO (1.5%) at 20°C with agitation.

805 At least 3 independent assays were carried out and the combined data was analyzed by
806 *t-test* using GraphPad Prism software (version 5.0a).

807 **Lifespan Analysis**

808 All lifespans were performed at 20°C. Semi-synchronized eggs were obtained by
809 hypochlorite treatment of adult hermaphrodites and placed on NGM plates seeded with
810 HT115 *E. coli* bacteria. During the course of the lifespan assays, we transferred adult
811 worms to fresh plates every day during their reproductive period and afterwards on
812 alternate days. Worms were scored as dead when they no longer responded to touch,
813 while exploded animals, those exhibiting bagging (embryo hatching inside the worm), or
814 dried out at the edges of the plates were censored.

815 For N-Acetyl-L-Cysteine (NAC) (Sigma-Aldrich) treatments we added NAC to the RNAi
816 medium to a final concentration of 8 mM.

817 We used the GraphPad Prism software (version 5.0a) to plot survival curves and to
818 determine significant differences in lifespans (log-rank (Mantel-Cox) test). See Table S1
819 for lifespan statistics.

820 **RNAi screen**

821 We performed an image-based RNAi screen as previously described(Hernando-
822 Rodriguez et al., 2018). Briefly, we dispensed synchronized *sgk-1(ok538);*P*hsp-6*::GFP
823 L1 larvae in 96 well plates using a microplate dispenser (EL406 washer dispenser,
824 BioTek) and added the corresponding dsRNA encoding bacterial culture. Next, we
825 incubated the worms at 20°C with constant shaking (120 rpm - New Brunswick™
826 Innova® 44/44R) until they reached the young adult stage. We acquired pictures of each
827 well using the IN Cell Analyzer 2000 (GE Healthcare) and performed the image analysis
828 with a user-defined protocol which was developed on the Developer Toolbox software
829 (GE Healthcare). We tested 836 RNAi clones in duplicate and candidates were defined
830 based on the adjusted *p* value and the fold change (FC) (P value < 0.001 and FC < 0.6).

Acknowledgements

Some strains were provided by the Caenorhabditis Genetics Center (CGC), which is funded by NIH Office of Research Infrastructure Programs (P40 OD010440). Special thanks to Ralf Baumeister (Albert-Ludwig University, Germany) for the strain BR2773:*byEx*[*Psgk-1::*SGK-1*::*GFP] (Hertweck et al., 2004) and to Nuria Flames for sharing her transcription factor RNAi library. Thanks to Mario Soriano Navarro, from the CIPF, for technical help with TEM. M.A-S was supported by the Ramón y Cajal program of the Spanish Ministerio de Economía y Competitividad (MINECO), RYC-2010-06167. B.H.R. was supported by the Spanish MINECO FPI program, BES-2013-064047. Our work is supported by the Spanish Ministerio de Economía y Competitividad (BFU2012-35509), and the European Research Council (ERC-2011-StG-281691).

Author contributions

B.H.R., M.M.P.J. and M.A.-S. designed the experiments; B.H.R., M.M.P.J., M.J.R.-P. A.P., M.D.M.-B. P.dl.C.R., R.G. and M.A.-S. carried out experiments; B.H.R., M.M.P.J., M.J.R.-P. A.P., M.D.M.-B. P.dl.C.R., R.G. and M.A.-S analyzed the data and interpreted results and B.H.R. and M.A.-S wrote the manuscript. All authors read, commented and approved the final manuscript.

Competing interests

The authors declare no competing financial interests.

References

Ackema, K.B., J. Hench, S. Bockler, S.C. Wang, U. Sauder, H. Mergentaler, B. Westermann, F. Bard, S. Frank, and A. Spang. 2014. The small GTPase Arf1 modulates mitochondrial morphology and function. *EMBO J.* 33:2659-2675.

Ackema, K.B., U. Sauder, J.A. Solinger, and A. Spang. 2013. The ArfGEF GBF-1 Is Required for ER Structure, Secretion and Endocytic Transport in C. elegans. *PLoS One*. 8:e67076.

857 Admasu, T.D., K. Chaithanya Batchu, D. Barardo, L.F. Ng, V.Y.M. Lam, L. Xiao, A.
858 Cazenave-Gassiot, M.R. Wenk, N.S. Tolwinski, and J. Gruber. 2018. Drug Synergy
859 Slows Aging and Improves Healthspan through IGF and SREBP Lipid Signaling. *Dev*
860 *Cell*. 47:67-79 e65.
861 Andres-Mateos, E., H. Brinkmeier, T.N. Burks, R. Mejias, D.C. Files, M. Steinberger, A.
862 Soleimani, R. Marx, J.L. Simmers, B. Lin, E. Finanger Hedderick, T.G. Marr, B.M. Lin,
863 C. Hourde, L.A. Leinwand, D. Kuhl, M. Foller, S. Vogelsang, I. Hernandez-Diaz, D.K.
864 Vaughan, D. Alvarez de la Rosa, F. Lang, and R.D. Cohn. 2013. Activation of
865 serum/glucocorticoid-induced kinase 1 (SGK1) is important to maintain skeletal
866 muscle homeostasis and prevent atrophy. *EMBO Mol Med*. 5:80-91.
867 Ardail, D., I. Popa, J. Bodennec, P. Louisot, D. Schmitt, and J. Portoukalian. 2003. The
868 mitochondria-associated endoplasmic-reticulum subcompartment (MAM fraction) of
869 rat liver contains highly active sphingolipid-specific glycosyltransferases. *Biochem J*.
870 371:1013-1019.
871 Artal-Sanz, M., and N. Tavernarakis. 2009a. Prohibitin and mitochondrial biology. *Trends*
872 *Endocrinol Metab*. 20:394-401.
873 Artal-Sanz, M., and N. Tavernarakis. 2009b. Prohibitin couples diapause signalling to
874 mitochondrial metabolism during ageing in C. elegans. *Nature*. 461:793-797.
875 Artal-Sanz, M., W.Y. Tsang, E.M. Willems, L.A. Grivell, B.D. Lemire, H. van der Spek,
876 and L.G. Nijtmans. 2003. The mitochondrial prohibitin complex is essential for
877 embryonic viability and germline function in Caenorhabditis elegans. *J Biol Chem*.
878 278:32091-32099.
879 Aspernig, H., T. Heimbucher, W. Qi, D. Gangurde, S. Curic, Y. Yan, E. Donner von
880 Gromoff, R. Baumeister, and A. Thien. 2019. Mitochondrial Perturbations Couple
881 mTORC2 to Autophagy in C. elegans. *Cell Rep*. 29:1399-1409 e1395.
882 Balklava, Z., S. Pant, H. Fares, and B.D. Grant. 2007. Genome-wide analysis identifies
883 a general requirement for polarity proteins in endocytic traffic. *Nat Cell Biol*. 9:1066-
884 1073.
885 Benedetti, C., C.M. Haynes, Y. Yang, H.P. Harding, and D. Ron. 2006. Ubiquitin-like
886 protein 5 positively regulates chaperone gene expression in the mitochondrial
887 unfolded protein response. *Genetics*. 174:229-239.
888 Berchtold, D., M. Piccolis, N. Chiaruttini, I. Riezman, H. Riezman, A. Roux, T.C. Walther,
889 and R. Loewith. 2012. Plasma membrane stress induces relocalization of Slm
890 proteins and activation of TORC2 to promote sphingolipid synthesis. *Nat Cell Biol*.
891 14:542-547.
892 Betz, C., and M.N. Hall. 2013. Where is mTOR and what is it doing there? *J Cell Biol*.
893 203:563-574.
894 Betz, C., D. Stracka, C. Prescianotto-Baschong, M. Frieden, N. Demaurex, and M.N.
895 Hall. 2013. Feature Article: mTOR complex 2-Akt signaling at mitochondria-
896 associated endoplasmic reticulum membranes (MAM) regulates mitochondrial
897 physiology. *Proc Natl Acad Sci U S A*. 110:12526-12534.
898 Bionda, C., J. Portoukalian, D. Schmitt, C. Rodriguez-Lafrasse, and D. Ardail. 2004.
899 Subcellular compartmentalization of ceramide metabolism: MAM (mitochondria-
900 associated membrane) and/or mitochondria? *Biochem J*. 382:527-533.
901 Birner, R., R. Nebauer, R. Schneiter, and G. Daum. 2003. Synthetic lethal interaction of
902 the mitochondrial phosphatidylethanolamine biosynthetic machinery with the
903 prohibitin complex of Saccharomyces cerevisiae. *Mol Biol Cell*. 14:370-383.
904 Bomberger, J.M., B.A. Coutermarsh, R.L. Barnaby, J.D. Sato, M.C. Chapline, and B.A.
905 Stanton. 2014. Serum and glucocorticoid-inducible kinase1 increases plasma
906 membrane wt-CFTR in human airway epithelial cells by inhibiting its endocytic
907 retrieval. *PLoS One*. 9:e89599.
908 Bourgoint, C., D. Rispal, M. Berti, I. Filipuzzi, S.B. Helliwell, M. Prouteau, and R. Loewith.
909 2018. Target of rapamycin complex 2-dependent phosphorylation of the coat protein

910 Pan1 by Akl1 controls endocytosis dynamics in Saccharomyces cerevisiae. *J Biol*
911 *Chem*. 293:12043-12053.
912 Brenner, S. 1974. The genetics of Caenorhabditis elegans. *Genetics*. 77:71-94.
913 Brodsky, J.L., and E.A. Fisher. 2008. The many intersecting pathways underlying
914 apolipoprotein B secretion and degradation. *Trends Endocrinol Metab*. 19:254-259.
915 Brown, M.S., and J.L. Goldstein. 1997. The SREBP pathway: regulation of cholesterol
916 metabolism by proteolysis of a membrane-bound transcription factor. *Cell*. 89:331-
917 340.
918 Chamoli, M., A. Singh, Y. Malik, and A. Mukhopadhyay. 2014. A novel kinase regulates
919 dietary restriction-mediated longevity in Caenorhabditis elegans. *Aging Cell*. 13:641-
920 655.
921 Chang, J.T., C. Kumsta, A.B. Hellman, L.M. Adams, and M. Hansen. 2017.
922 Spatiotemporal regulation of autophagy during Caenorhabditis elegans aging. *Elife*.
923 6.
924 Chen, A.T., C. Guo, K.J. Dumas, K. Ashrafi, and P.J. Hu. 2013. Effects of Caenorhabditis
925 elegans sgk-1 mutations on lifespan, stress resistance, and DAF-16/FoxO regulation.
926 *Aging Cell*. 12:932-940.
927 Clarke, J., N. Dephoure, I. Horecka, S. Gygi, and D. Kellogg. 2017. A conserved
928 signaling network monitors delivery of sphingolipids to the plasma membrane in
929 budding yeast. *Mol Biol Cell*. 28:2589-2599.
930 Csordas, G., A.P. Thomas, and G. Hajnoczky. 1999. Quasi-synaptic calcium signal
931 transmission between endoplasmic reticulum and mitochondria. *EMBO J*. 18:96-108.
932 Cutler, R.G., K.W. Thompson, S. Camandola, K.T. Mack, and M.P. Mattson. 2014.
933 Sphingolipid metabolism regulates development and lifespan in Caenorhabditis
934 elegans. *Mech Ageing Dev*. 143-144:9-18.
935 deHart, A.K., J.D. Schnell, D.A. Allen, and L. Hicke. 2002. The conserved Pkh-Ypk
936 kinase cascade is required for endocytosis in yeast. *J Cell Biol*. 156:241-248.
937 Di Cristofano, A. 2017. SGK1: The Dark Side of PI3K Signaling. *Curr Top Dev Biol*.
938 123:49-71.
939 Dillin, A., A.L. Hsu, N. Arantes-Oliveira, J. Lehrer-Graiwer, H. Hsin, A.G. Fraser, R.S.
940 Kamath, J. Ahringer, and C. Kenyon. 2002. Rates of behavior and aging specified by
941 mitochondrial function during development. *Science*. 298:2398-2401.
942 Dowen, R.H., P.C. Breen, T. Tullius, A.L. Conery, and G. Ruvkun. 2016. A microRNA
943 program in the C. elegans hypodermis couples to intestinal mTORC2/PQM-1
944 signaling to modulate fat transport. *Genes Dev*. 30:1515-1528.
945 Ezcurra, M., A. Benedetto, T. Sornda, A.F. Gilliat, C. Au, Q. Zhang, S. van Schelt, A.L.
946 Petrache, H. Wang, Y. de la Guardia, S. Bar-Nun, E. Tyler, M.J. Wakelam, and D.
947 Gems. 2018. C. elegans Eats Its Own Intestine to Make Yolk Leading to Multiple
948 Senescent Pathologies. *Curr Biol*. 28:2544-2556 e2545.
949 Fang, E.F., T.B. Waltz, H. Kassahun, Q. Lu, J.S. Kerr, M. Morevati, E.M. Fivenson, B.N.
950 Wollman, K. Marosi, M.A. Wilson, W.B. Iser, D.M. Eckley, Y. Zhang, E. Lehrmann,
951 I.G. Goldberg, M. Scheibye-Knudsen, M.P. Mattson, H. Nilsen, V.A. Bohr, and K.G.
952 Becker. 2017. Tomatidine enhances lifespan and healthspan in C. elegans through
953 mitophagy induction via the SKN-1/Nrf2 pathway. *Sci Rep*. 7:46208.
954 Fujimoto, M., T. Hayashi, and T.P. Su. 2012. The role of cholesterol in the association
955 of endoplasmic reticulum membranes with mitochondria. *Biochem Biophys Res*
956 *Commun*. 417:635-639.
957 Gatsi, R., B. Schulze, M.J. Rodriguez-Palero, B. Hernando-Rodriguez, R. Baumeister,
958 and M. Artal-Sanz. 2014. Prohibitin-mediated lifespan and mitochondrial stress
959 implicate SGK-1, insulin/IGF and mTORC2 in C. elegans. *PLoS One*. 9:e107671.
960 Goldstein, J.L., R.A. DeBose-Boyd, and M.S. Brown. 2006. Protein sensors for
961 membrane sterols. *Cell*. 124:35-46.

962 Gosai, S.J., J.H. Kwak, C.J. Luke, O.S. Long, D.E. King, K.J. Kovatch, P.A. Johnston,
963 T.Y. Shun, J.S. Lazo, D.H. Perlmutter, G.A. Silverman, and S.C. Pak. 2010.
964 Automated high-content live animal drug screening using C. elegans expressing the
965 aggregation prone serpin alpha1-antitrypsin Z. *PLoS One*. 5:e15460.
966 Hagiwara, A., M. Cornu, N. Cybulski, P. Polak, C. Betz, F. Trapani, L. Terracciano, M.H.
967 Heim, M.A. Ruegg, and M.N. Hall. 2012. Hepatic mTORC2 activates glycolysis and
968 lipogenesis through Akt, glucokinase, and SREBP1c. *Cell Metab*. 15:725-738.
969 Hall, D.H., E. Hartwieg, and K.C. Nguyen. 2012. Modern electron microscopy methods
970 for C. elegans. *Methods Cell Biol*. 107:93-149.
971 Hamasaki, M., N. Furuta, A. Matsuda, A. Nezu, A. Yamamoto, N. Fujita, H. Oomori, T.
972 Noda, T. Haraguchi, Y. Hiraoka, A. Amano, and T. Yoshimori. 2013. Autophagosomes
973 form at ER-mitochondria contact sites. *Nature*. 495:389-393.
974 Hernando-Rodriguez, B., A.P. Erinjeri, M.J. Rodriguez-Palero, V. Millar, S. Gonzalez-
975 Hernandez, M. Olmedo, B. Schulze, R. Baumeister, M.J. Munoz, P. Askjaer, and M.
976 Artal-Sanz. 2018. Combined flow cytometry and high-throughput image analysis for
977 the study of essential genes in Caenorhabditis elegans. *BMC Biol*. 16:36.
978 Hertweck, M., C. Gobel, and R. Baumeister. 2004. C. elegans SGK-1 is the critical
979 component in the Akt/PKB kinase complex to control stress response and life span.
980 *Dev Cell*. 6:577-588.
981 Horton, J.D., J.L. Goldstein, and M.S. Brown. 2002. SREBPs: activators of the complete
982 program of cholesterol and fatty acid synthesis in the liver. *J Clin Invest*. 109:1125-
983 1131.
984 Hwang, A.B., E.A. Ryu, M. Artan, H.W. Chang, M.H. Kabir, H.J. Nam, D. Lee, J.S. Yang,
985 S. Kim, W.B. Mair, C. Lee, S.S. Lee, and S.J. Lee. 2014. Feedback regulation via
986 AMPK and HIF-1 mediates ROS-dependent longevity in Caenorhabditis elegans.
987 *Proc Natl Acad Sci U S A*. 111:E4458-4467.
988 Jones, K.T., E.R. Greer, D. Pearce, and K. Ashrafi. 2009. Rictor/TORC2 regulates
989 Caenorhabditis elegans fat storage, body size, and development through sgk-1. *PLoS*
990 *Biol*. 7:e60.
991 Kaczmarek, B., J.M. Verbavatz, and C.L. Jackson. 2017. GBF1 and Arf1 function in
992 vesicular trafficking, lipid homoeostasis and organelle dynamics. *Biol Cell*. 109:391-
993 399.
994 Kamal, M., D.R. D'Amora, and T.J. Kubiseski. 2016. Loss of hif-1 promotes resistance
995 to the exogenous mitochondrial stressor ethidium bromide in Caenorhabditis elegans.
996 *BMC Cell Biol*. 17 Suppl 1:34.
997 Kim, S., and D. Sieburth. 2018. Sphingosine Kinase Activates the Mitochondrial
998 Unfolded Protein Response and Is Targeted to Mitochondria by Stress. *Cell Rep*.
999 24:2932-2945 e2934.
1000 Kimura, S., T. Noda, and T. Yoshimori. 2007. Dissection of the autophagosome
1001 maturation process by a novel reporter protein, tandem fluorescent-tagged LC3.
1002 *Autophagy*. 3:452-460.
1003 Kirienko, N.V., F.M. Ausubel, and G. Ruvkun. 2015. Mitophagy confers resistance to
1004 siderophore-mediated killing by Pseudomonas aeruginosa. *Proc Natl Acad Sci U S*
1005 *A*. 112:1821-1826.
1006 Klecker, T., M. Wemmer, M. Haag, A. Weig, S. Bockler, T. Langer, J. Nunnari, and B.
1007 Westermann. 2015. Interaction of MDM33 with mitochondrial inner membrane
1008 homeostasis pathways in yeast. *Sci Rep*. 5:18344.
1009 Kornmann, B., E. Currie, S.R. Collins, M. Schuldiner, J. Nunnari, J.S. Weissman, and P.
1010 Walter. 2009. An ER-mitochondria tethering complex revealed by a synthetic biology
1011 screen. *Science*. 325:477-481.
1012 Krueger, B., S. Haerteis, L. Yang, A. Hartner, R. Rauh, C. Korbmacher, and A. Diakov.
1013 2009. Cholesterol depletion of the plasma membrane prevents activation of the
1014 epithelial sodium channel (ENaC) by SGK1. *Cell Physiol Biochem*. 24:605-618.

1015 Labbadia, J., R.M. Brielmann, M.F. Neto, Y.F. Lin, C.M. Haynes, and R.I. Morimoto.
1016 2017. Mitochondrial Stress Restores the Heat Shock Response and Prevents
1017 Proteostasis Collapse during Aging. *Cell Rep*. 21:1481-1494.
1018 Lapierre, L.R., C.D. De Magalhaes Filho, P.R. McQuary, C.C. Chu, O. Visvikis, J.T.
1019 Chang, S. Gelino, B. Ong, A.E. Davis, J.E. Irazoqui, A. Dillin, and M. Hansen. 2013.
1020 The TFEB orthologue HLH-30 regulates autophagy and modulates longevity in
1021 Caenorhabditis elegans. *Nat Commun*. 4:2267.
1022 Lee, S.J., A.B. Hwang, and C. Kenyon. 2010. Inhibition of respiration extends C. elegans
1023 life span via reactive oxygen species that increase HIF-1 activity. *Curr Biol*. 20:2131-
1024 2136.
1025 Lehmann, S., J.J. Bass, and N.J. Szewczyk. 2013. Knockdown of the C. elegans kinome
1026 identifies kinases required for normal protein homeostasis, mitochondrial network
1027 structure, and sarcomere structure in muscle. *Cell Commun Signal*. 11:71.
1028 Lev, I., R. Bril, Y. Liu, L.I. Cere, and O. Rechavi. 2019. Inter-generational consequences
1029 for growing Caenorhabditis elegans in liquid. *Philos Trans R Soc Lond B Biol Sci*.
1030 374:20180125.
1031 Liu, Y., B.S. Samuel, P.C. Breen, and G. Ruvkun. 2014. Caenorhabditis elegans
1032 pathways that surveil and defend mitochondria. *Nature*. 508:406-410.
1033 Lucena, R., M. Alcaide-Gavilan, K. Schubert, M. He, M.G. Domnauer, C. Marquer, C.
1034 Klose, M.A. Surma, and D.R. Kellogg. 2018. Cell Size and Growth Rate Are
1035 Modulated by TORC2-Dependent Signals. *Curr Biol*. 28:196-210 e194.
1036 Luz, A.L., J.P. Rooney, L.L. Kubik, C.P. Gonzalez, D.H. Song, and J.N. Meyer. 2015.
1037 Mitochondrial Morphology and Fundamental Parameters of the Mitochondrial
1038 Respiratory Chain Are Altered in Caenorhabditis elegans Strains Deficient in
1039 Mitochondrial Dynamics and Homeostasis Processes. *PLoS One*. 10:e0130940.
1040 Magner, D.B., J. Wollam, Y. Shen, C. Hoppe, D. Li, C. Latza, V. Rottiers, H. Hutter, and
1041 A. Antebi. 2013. The NHR-8 nuclear receptor regulates cholesterol and bile acid
1042 homeostasis in C. elegans. *Cell Metab*. 18:212-224.
1043 Marks, G.L., and D.O. Wood. 1992. Nucleotide sequence of the Rickettsia prowazekii
1044 greA homolog. *Nucleic Acids Res*. 20:3785.
1045 Melendez, A., and B. Levine. 2009. Autophagy in C. elegans. *WormBook*:1-26.
1046 Menuz, V., K.S. Howell, S. Gentina, S. Epstein, I. Riezman, M. Fornallaz-Mulhauser,
1047 M.O. Hengartner, M. Gomez, H. Riezman, and J.C. Martinou. 2009. Protection of C.
1048 elegans from anoxia by HYL-2 ceramide synthase. *Science*. 324:381-384.
1049 Merkwirth, C., and T. Langer. 2009. Prohibitin function within mitochondria: essential
1050 roles for cell proliferation and cristae morphogenesis. *Biochim Biophys Acta*. 1793:27-
1051 32.
1052 Merkwirth, C., P. Martinelli, A. Korwitz, M. Morbin, H.S. Bronneke, S.D. Jordan, E.I.
1053 Rugarli, and T. Langer. 2012. Loss of prohibitin membrane scaffolds impairs
1054 mitochondrial architecture and leads to tau hyperphosphorylation and
1055 neurodegeneration. *PLoS Genet*. 8:e1003021.
1056 Mizunuma, M., E. Neumann-Haefelin, N. Moroz, Y. Li, and T.K. Blackwell. 2014.
1057 mTORC2-SGK-1 acts in two environmentally responsive pathways with opposing
1058 effects on longevity. *Aging Cell*. 13:869-878.
1059 Mosbech, M.B., R. Kruse, E.B. Harvald, A.S. Olsen, S.F. Gallego, H.K. Hannibal-Bach,
1060 C.S. Ejsing, and N.J. Faergeman. 2013. Functional loss of two ceramide synthases
1061 elicits autophagy-dependent lifespan extension in C. elegans. *PLoS One*. 8:e70087.
1062 Mouchiroud, L., R.H. Houtkooper, N. Moullan, E. Katsyuba, D. Ryu, C. Canto, A. Mottis,
1063 Y.S. Jo, M. Viswanathan, K. Schoonjans, L. Guarente, and J. Auwerx. 2013. The
1064 NAD(+)/Sirtuin Pathway Modulates Longevity through Activation of Mitochondrial
1065 UPR and FOXO Signaling. *Cell*. 154:430-441.

1066 Muir, A., S. Ramachandran, F.M. Roelants, G. Timmons, and J. Thorner. 2014. TORC2-
1067 dependent protein kinase Ypk1 phosphorylates ceramide synthase to stimulate
1068 synthesis of complex sphingolipids. *Elife*. 3.
1069 Murley, A., J. Yamada, B.J. Niles, A. Toulmay, W.A. Prinz, T. Powers, and J. Nunnari.
1070 2017. Sterol transporters at membrane contact sites regulate TORC1 and TORC2
1071 signaling. *J Cell Biol*. 216:2679-2689.
1072 Narendra, D.P., and R.J. Youle. 2011. Targeting mitochondrial dysfunction: role for
1073 PINK1 and Parkin in mitochondrial quality control. *Antioxid Redox Signal*. 14:1929-
1074 1938.
1075 Nargund, A.M., C.J. Fiorese, M.W. Pellegrino, P. Deng, and C.M. Haynes. 2015.
1076 Mitochondrial and nuclear accumulation of the transcription factor ATFS-1 promotes
1077 OXPHOS recovery during the UPR(mt). *Mol Cell*. 58:123-133.
1078 Nijtmans, L.G., S.M. Artal, L.A. Grivell, and P.J. Coates. 2002. The mitochondrial PHB
1079 complex: roles in mitochondrial respiratory complex assembly, ageing and
1080 degenerative disease. *Cell Mol Life Sci*. 59:143-155.
1081 Nijtmans, L.G., L. de Jong, M. Artal Sanz, P.J. Coates, J.A. Berden, J.W. Back, A.O.
1082 Muijsers, H. van der Spek, and L.A. Grivell. 2000. Prohibitins act as a membrane-
1083 bound chaperone for the stabilization of mitochondrial proteins. *EMBO J*. 19:2444-
1084 2451.
1085 Niles, B.J., A.C. Joslin, T. Fresques, and T. Powers. 2014. TOR complex 2-Ypk1
1086 signaling maintains sphingolipid homeostasis by sensing and regulating ROS
1087 accumulation. *Cell Rep*. 6:541-552.
1088 Nomura, T., M. Horikawa, S. Shimamura, T. Hashimoto, and K. Sakamoto. 2010. Fat
1089 accumulation in Caenorhabditis elegans is mediated by SREBP homolog SBP-1.
1090 *Genes Nutr*. 5:17-27.
1091 O'Keeffe, B.A., S. Cilia, A.C. Maiyar, M. Vaysberg, and G.L. Firestone. 2013. The serum-
1092 and glucocorticoid-induced protein kinase-1 (Sgk-1) mitochondria connection:
1093 identification of the IF-1 inhibitor of the F(1)F(0)-ATPase as a mitochondria-specific
1094 binding target and the stress-induced mitochondrial localization of endogenous Sgk-
1095 1. *Biochimie*. 95:1258-1265.
1096 Osman, C., M. Haag, C. Potting, J. Rodenfels, P.V. Dip, F.T. Wieland, B. Brugger, B.
1097 Westermann, and T. Langer. 2009. The genetic interactome of prohibitins:
1098 coordinated control of cardiolipin and phosphatidylethanolamine by conserved
1099 regulators in mitochondria. *J Cell Biol*. 184:583-596.
1100 Palikaras, K., E. Lionaki, and N. Tavernarakis. 2015. Coordination of mitophagy and
1101 mitochondrial biogenesis during ageing in C. elegans. *Nature*. 521:525-528.
1102 Perry, R.J., and N.D. Ridgway. 2005. Molecular mechanisms and regulation of ceramide
1103 transport. *Biochim Biophys Acta*. 1734:220-234.
1104 Raturi, A., and T. Simmen. 2013. Where the endoplasmic reticulum and the
1105 mitochondrion tie the knot: the mitochondria-associated membrane (MAM). *Biochim*
1106 *Biophys Acta*. 1833:213-224.
1107 Richter-Dennerlein, R., A. Korwitz, M. Haag, T. Tatsuta, S. Dargazanli, M. Baker, T.
1108 Decker, T. Lamkemeyer, E.I. Rugarli, and T. Langer. 2014. DNAJC19, a mitochondrial
1109 cochaperone associated with cardiomyopathy, forms a complex with prohibitins to
1110 regulate cardiolipin remodeling. *Cell Metab*. 20:158-171.
1111 Rizzuto, R., P. Pinton, W. Carrington, F.S. Fay, K.E. Fogarty, L.M. Lifshitz, R.A. Tuft, and
1112 T. Pozzan. 1998. Close contacts with the endoplasmic reticulum as determinants of
1113 mitochondrial Ca2+ responses. *Science*. 280:1763-1766.
1114 Roelants, F.M., D.K. Breslow, A. Muir, J.S. Weissman, and J. Thorner. 2011. Protein
1115 kinase Ypk1 phosphorylates regulatory proteins Orm1 and Orm2 to control
1116 sphingolipid homeostasis in Saccharomyces cerevisiae. *Proc Natl Acad Sci U S A*.
1117 108:19222-19227.

1118 Roelants, F.M., N. Chauhan, A. Muir, J.C. Davis, A.K. Menon, T.P. Levine, and J.
1119 Thorner. 2018. TOR complex 2-regulated protein kinase Ypk1 controls sterol
1120 distribution by inhibiting StARkin domain-containing proteins located at plasma
1121 membrane-endoplasmic reticulum contact sites. *Mol Biol Cell*. 29:2128-2136.
1122 Salo, V.T., and E. Ikonen. 2019. Moving out but keeping in touch: contacts between
1123 endoplasmic reticulum and lipid droplets. *Curr Opin Cell Biol*. 57:64-70.
1124 Schaar, C.E., D.J. Dues, K.K. Spielbauer, E. Machiela, J.F. Cooper, M. Senchuk, S.
1125 Hekimi, and J.M. Van Raamsdonk. 2015. Mitochondrial and cytoplasmic ROS have
1126 opposing effects on lifespan. *PLoS Genet*. 11:e1004972.
1127 Schiavi, A., A. Torgovnick, A. Kell, E. Megalou, N. Castelein, I. Guccini, L. Marzocchella,
1128 S. Gelino, M. Hansen, F. Malisan, I. Condo, R. Bei, S.L. Rea, B.P. Braeckman, N.
1129 Tavernarakis, R. Testi, and N. Ventura. 2013. Autophagy induction extends lifespan
1130 and reduces lipid content in response to frataxin silencing in C. elegans. *Exp Gerontol*.
1131 48:191-201.
1132 Schieke, S.M., D. Phillips, J.P. McCoy, Jr., A.M. Aponte, R.F. Shen, R.S. Balaban, and
1133 T. Finkel. 2006. The mammalian target of rapamycin (mTOR) pathway regulates
1134 mitochondrial oxygen consumption and oxidative capacity. *J Biol Chem*. 281:27643-
1135 27652.
1136 Senchuk, M.M., D.J. Dues, C.E. Schaar, B.K. Johnson, Z.B. Madaj, M.J. Bowman, M.E.
1137 Winn, and J.M. Van Raamsdonk. 2018. Activation of DAF-16/FOXO by reactive
1138 oxygen species contributes to longevity in long-lived mitochondrial mutants in
1139 Caenorhabditis elegans. *PLoS Genet*. 14:e1007268.
1140 Settembre, C., C. Di Malta, V.A. Polito, M. Garcia Arencibia, F. Vetrini, S. Erdin, S.U.
1141 Erdin, T. Huynh, D. Medina, P. Colella, M. Sardiello, D.C. Rubinsztein, and A.
1142 Ballabio. 2011. TFEB links autophagy to lysosomal biogenesis. *Science*. 332:1429-
1143 1433.
1144 Singh, P.K., S. Singh, and S. Ganesh. 2013. Activation of serum/glucocorticoid-induced
1145 kinase 1 (SGK1) underlies increased glycogen levels, mTOR activation, and
1146 autophagy defects in Lafora disease. *Mol Biol Cell*. 24:3776-3786.
1147 Smulan, L.J., W. Ding, E. Freinkman, S. Gujja, Y.J.K. Edwards, and A.K. Walker. 2016.
1148 Cholesterol-Independent SREBP-1 Maturation Is Linked to ARF1 Inactivation. *Cell*
1149 *Rep*. 16:9-18.
1150 Soukas, A.A., E.A. Kane, C.E. Carr, J.A. Melo, and G. Ruvkun. 2009. Rictor/TORC2
1151 regulates fat metabolism, feeding, growth, and life span in Caenorhabditis elegans.
1152 *Genes Dev*. 23:496-511.
1153 Stone, S.J., M.C. Levin, P. Zhou, J. Han, T.C. Walther, and R.V. Farese, Jr. 2009. The
1154 endoplasmic reticulum enzyme DGAT2 is found in mitochondria-associated
1155 membranes and has a mitochondrial targeting signal that promotes its association
1156 with mitochondria. *J Biol Chem*. 284:5352-5361.
1157 Strub, G.M., M. Paillard, J. Liang, L. Gomez, J.C. Allegood, N.C. Hait, M. Maceyka, M.M.
1158 Price, Q. Chen, D.C. Simpson, T. Kordula, S. Milstien, E.J. Lesnefsky, and S. Spiegel.
1159 2011. Sphingosine-1-phosphate produced by sphingosine kinase 2 in mitochondria
1160 interacts with prohibitin 2 to regulate complex IV assembly and respiration. *FASEB J*.
1161 25:600-612.
1162 Thondamal, M., M. Witting, P. Schmitt-Kopplin, and H. Aguilaniu. 2014. Steroid hormone
1163 signalling links reproduction to lifespan in dietary-restricted Caenorhabditis elegans.
1164 *Nat Commun*. 5:4879.
1165 Thuaud, F., N. Ribeiro, C.G. Nebigil, and L. Desaubry. 2013. Prohibitin ligands in cell
1166 death and survival: mode of action and therapeutic potential. *Chem Biol*. 20:316-331.
1167 Tian, Y., G. Garcia, Q. Bian, K.K. Steffen, L. Joe, S. Wolff, B.J. Meyer, and A. Dillin.
1168 2016. Mitochondrial Stress Induces Chromatin Reorganization to Promote Longevity
1169 and UPR(mt). *Cell*. 165:1197-1208.

1170 Toska, E., P. Castel, S. Chhangawala, A. Arruabarrena-Aristorena, C. Chan, V.C.
1171 Hristidis, E. Cocco, M. Sallaku, G. Xu, J. Park, G. Minuesa, S.G. Shifman, N.D. Socci,
1172 R. Koche, C.S. Leslie, M. Scaltriti, and J. Baselga. 2019. PI3K Inhibition Activates
1173 SGK1 via a Feedback Loop to Promote Chromatin-Based Regulation of ER-
1174 Dependent Gene Expression. *Cell Rep*. 27:294-306 e295.
1175 Toth, M.L., T. Sigmond, E. Borsos, J. Barna, P. Erdelyi, K. Takacs-Vellai, L. Orosz, A.L.
1176 Kovacs, G. Csikos, M. Sass, and T. Vellai. 2008. Longevity pathways converge on
1177 autophagy genes to regulate life span in Caenorhabditis elegans. *Autophagy*. 4:330-
1178 338.
1179 Tullet, J.M., M. Hertweck, J.H. An, J. Baker, J.Y. Hwang, S. Liu, R.P. Oliveira, R.
1180 Baumeister, and T.K. Blackwell. 2008. Direct inhibition of the longevity-promoting
1181 factor SKN-1 by insulin-like signaling in C. elegans. *Cell*. 132:1025-1038.
1182 van der Laan, M., M. Bohnert, N. Wiedemann, and N. Pfanner. 2012. Role of MINOS in
1183 mitochondrial membrane architecture and biogenesis. *Trends Cell Biol*. 22:185-192.
1184 Van Raamsdonk, J.M., and S. Hekimi. 2009. Deletion of the mitochondrial superoxide
1185 dismutase sod-2 extends lifespan in Caenorhabditis elegans. *PLoS Genet*.
1186 5:e1000361.
1187 Van Raamsdonk, J.M., Y. Meng, D. Camp, W. Yang, X. Jia, C. Benard, and S. Hekimi.
1188 2010. Decreased energy metabolism extends life span in Caenorhabditis elegans
1189 without reducing oxidative damage. *Genetics*. 185:559-571.
1190 Vance, J.E. 1990. Phospholipid synthesis in a membrane fraction associated with
1191 mitochondria. *J Biol Chem*. 265:7248-7256.
1192 Ventura, N., S.L. Rea, and R. Testi. 2006. Long-lived C. elegans mitochondrial mutants
1193 as a model for human mitochondrial-associated diseases. *Exp Gerontol*. 41:974-991.
1194 Verfaillie, T., N. Rubio, A.D. Garg, G. Bultynck, R. Rizzuto, J.P. Decuypere, J. Piette, C.
1195 Linehan, S. Gupta, A. Samali, and P. Agostinis. 2012. PERK is required at the ER-
1196 mitochondrial contact sites to convey apoptosis after ROS-based ER stress. *Cell*
1197 *Death Differ*. 19:1880-1891.
1198 Vlahakis, A., M. Graef, J. Nunnari, and T. Powers. 2014. TOR complex 2-Ypk1 signaling
1199 is an essential positive regulator of the general amino acid control response and
1200 autophagy. *Proc Natl Acad Sci U S A*. 111:10586-10591.
1201 Vlahakis, A., N. Lopez Muniozguren, and T. Powers. 2016. Calcium channel regulator
1202 Mid1 links TORC2-mediated changes in mitochondrial respiration to autophagy. *J Cell*
1203 *Biol*. 215:779-788.
1204 Vlahakis, A., N. Lopez Muniozguren, and T. Powers. 2017. Stress-response transcription
1205 factors Msn2 and Msn4 couple TORC2-Ypk1 signaling and mitochondrial respiration
1206 to ATG8 gene expression and autophagy. *Autophagy*. 13:1804-1812.
1207 Walker, A.K., R.L. Jacobs, J.L. Watts, V. Rottiers, K. Jiang, D.M. Finnegan, T. Shioda,
1208 M. Hansen, F. Yang, L.J. Niebergall, D.E. Vance, M. Tzoneva, A.C. Hart, and A.M.
1209 Naar. 2011. A conserved SREBP-1/phosphatidylcholine feedback circuit regulates
1210 lipogenesis in metazoans. *Cell*. 147:840-852.
1211 Wang, H., X. Jiang, J. Wu, L. Zhang, J. Huang, Y. Zhang, X. Zou, and B. Liang. 2016.
1212 Iron Overload Coordinately Promotes Ferritin Expression and Fat Accumulation in
1213 Caenorhabditis elegans. *Genetics*. 203:241-253.
1214 Wang, M., Y. Xue, L. Shen, P. Qin, X. Sang, Z. Tao, J. Yi, J. Wang, P. Liu, and H. Cheng.
1215 2019. Inhibition of SGK1 confers vulnerability to redox dysregulation in cervical
1216 cancer. *Redox Biol*. 24:101225.
1217 Wei, Y., M. Liu, X. Li, J. Liu, and H. Li. 2018. Origin of the Autophagosome Membrane
1218 in Mammals. *Biomed Res Int*. 2018:1012789.
1219 Wilkinson, M.F. 2019. Genetic paradox explained by nonsense. *Nature*. 568:179-180.
1220 Wu, H., P. Carvalho, and G.K. Voeltz. 2018a. Here, there, and everywhere: The
1221 importance of ER membrane contact sites. *Science*. 361.

1222 Wu, Z., M.M. Senchuk, D.J. Dues, B.K. Johnson, J.F. Cooper, L. Lew, E. Machiela, C.E.
1223 Schaar, H. DeJonge, T.K. Blackwell, and J.M. Van Raamsdonk. 2018b. Mitochondrial
1224 unfolded protein response transcription factor ATFS-1 promotes longevity in a long-
1225 lived mitochondrial mutant through activation of stress response pathways. *BMC Biol*.
1226 16:147.
1227 Yang, W., and S. Hekimi. 2010. A mitochondrial superoxide signal triggers increased
1228 longevity in Caenorhabditis elegans. *PLoS Biol*. 8:e1000556.
1229 Yen, K., T.T. Le, A. Bansal, S.D. Narasimhan, J.X. Cheng, and H.A. Tissenbaum. 2010.
1230 A comparative study of fat storage quantitation in nematode Caenorhabditis elegans
1231 using label and label-free methods. *PLoS One*. 5.
1232 Yoneda, T., C. Benedetti, F. Urano, S.G. Clark, H.P. Harding, and D. Ron. 2004.
1233 Compartment-specific perturbation of protein handling activates genes encoding
1234 mitochondrial chaperones. *J Cell Sci*. 117:4055-4066.
1235 Zhang, H., N. Abraham, L.A. Khan, D.H. Hall, J.T. Fleming, and V. Gobel. 2011.
1236 Apicobasal domain identities of expanding tubular membranes depend on
1237 glycosphingolipid biosynthesis. *Nat Cell Biol*. 13:1189-1201.
1238 Zhang, H., J.T. Chang, B. Guo, M. Hansen, K. Jia, A.L. Kovacs, C. Kumsta, L.R.
1239 Lapierre, R. Legouis, L. Lin, Q. Lu, A. Melendez, E.J. O'Rourke, K. Sato, M. Sato, X.
1240 Wang, and F. Wu. 2015. Guidelines for monitoring autophagy in Caenorhabditis
1241 elegans. *Autophagy*. 11:9-27.
1242 Zhou, B., J. Kreuzer, C. Kumsta, L. Wu, K.J. Kamer, L. Cedillo, Y. Zhang, S. Li, M.C.
1243 Kacergis, C.M. Webster, G. Fejes-Toth, A. Naray-Fejes-Toth, S. Das, M. Hansen, W.
1244 Haas, and A.A. Soukas. 2019. Mitochondrial Permeability Uncouples Elevated
1245 Autophagy and Lifespan Extension. *Cell*. 177:299-314 e216.
1246 Zhu, M., G. Wu, Y.X. Li, J.K. Stevens, C.X. Fan, A. Spang, and M.Q. Dong. 2015. Serum-
1247 and Glucocorticoid-Inducible Kinase-1 (SGK-1) Plays a Role in Membrane Trafficking
1248 in Caenorhabditis elegans. *PLoS One*. 10:e0130778.
1249

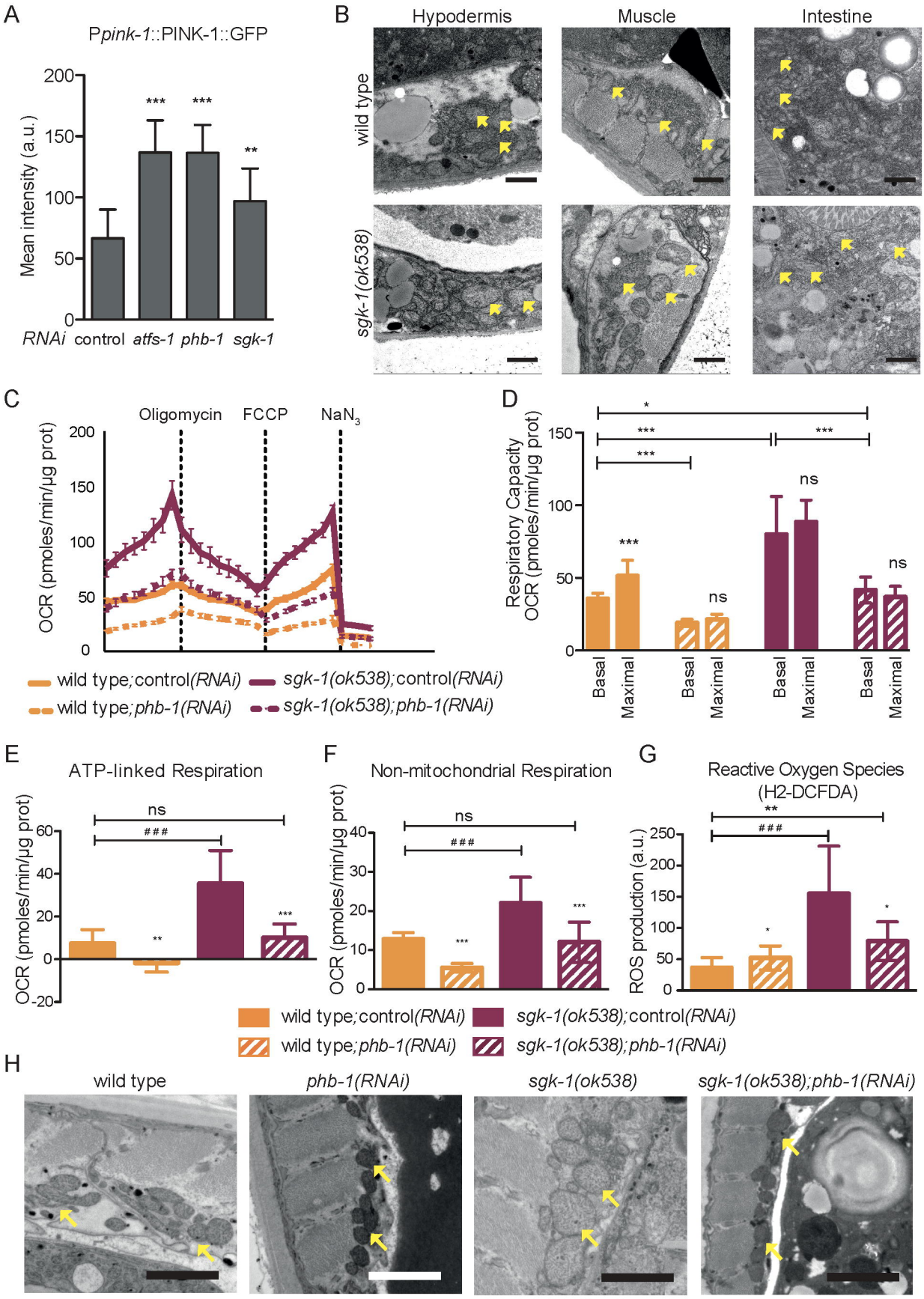

Figure 1: Prohibitin depletion suppresses the altered mitochondrial structure and function of *sgk-1* mutants. A. Quantification of P*pink-1*::PINK-1::GFP in worms treated with RNAi against *atfs-1*, *phb-1* and *sgk-1* at the young adult stage. **B.** Electron microscopy images of hypodermis, muscle and intestine of wild type and *sgk-1* mutants at day 1 of adulthood. Yellow arrows show mitochondria. Bar size: 1 µm. **C-F.** Seahorse measurements in wild type animals, *phb-1(RNAi)* treated worms, *sgk-1* mutants and *sgk-1;phb-1* depleted mutants at the young adult stage. **C.** Mitochondrial oxygen consumption rate. **D.** Basal and maximal respiratory capacity. **E.** ATP-linked respiration and **F.** Non-mitochondrial respiration. **G.** Reactive oxygen species (ROS) levels measured at the young adult stage of wild type animals, *phb-1(RNAi)* treated worms, *sgk-1* mutants and *sgk-1;phb-1* depleted mutants. **H.** Electron microscopy images of muscle cells, at day 5 of adulthood, of wild type and *sgk-1(ok538)* mutants under normal and mitochondrial stress conditions (*phb-1(RNAi)*). Yellow arrows point to mitochondria. Bar size: 1 µm. (Mean ± SD; *** p value < 0.001, ** p value < 0.01, * p value < 0.1, ns not significant compared against its respective *control(RNAi)*, ### p value < 0.001 compared against wild type *control(RNAi)*; *t-test*. Combination of three independent replicates).

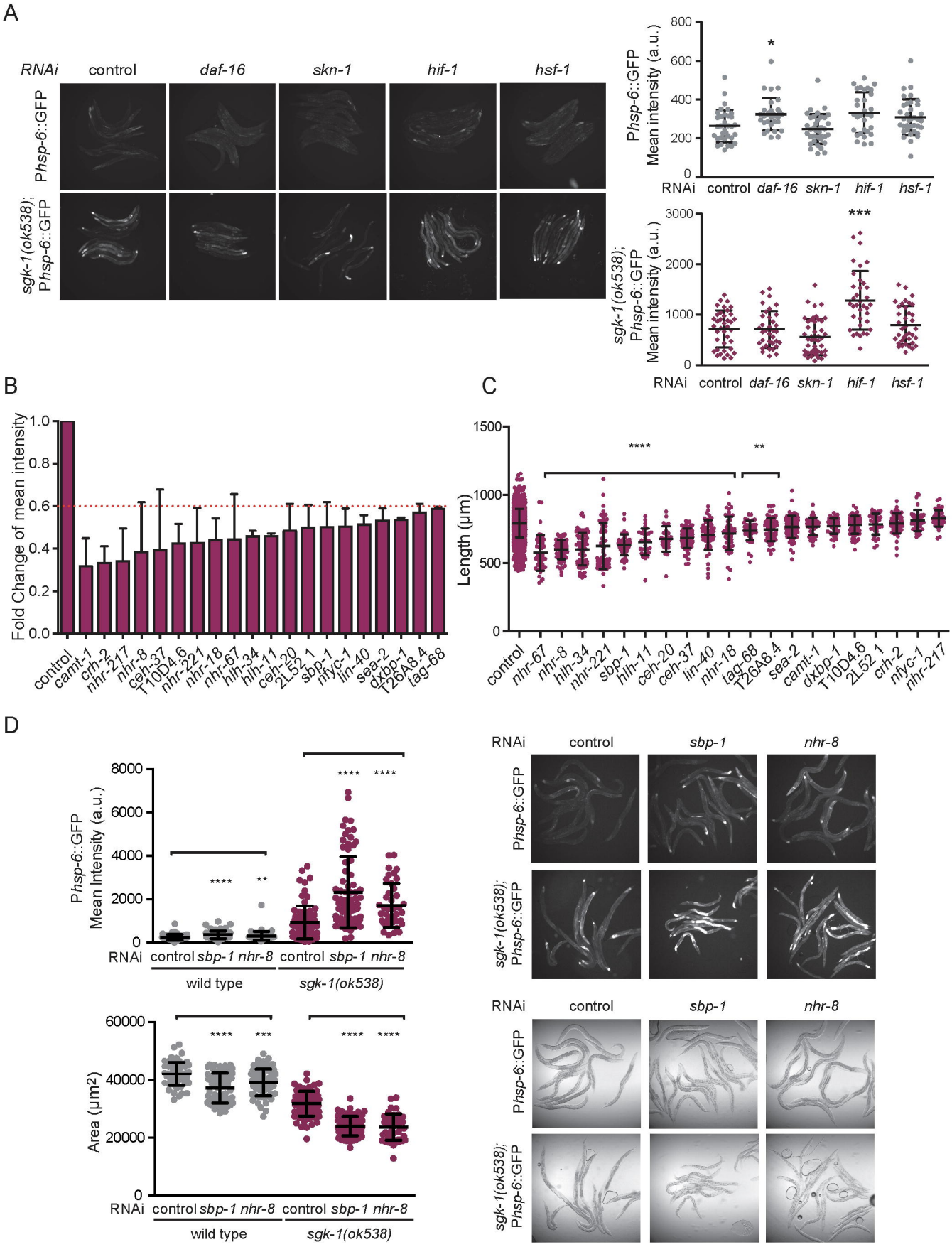

Figure 2: Altered membrane sterol and lipid homeostasis induces the UPR^{mt} in the TORC2/SGK-1 mutant. A. Quantification of the UPR^{mt} reporter P*hsp-6*::GFP in wild type animals (top) and *sgk-1* mutants (bottom) upon depletion of *daf-16, skn-1, hif-1* and *hsf-1*. (Mean ± SD; *** p value < 0.001, * p value < 0.1 compared against control(RNAi); ANOVA test). Representative images are shown. **B.** Fold change of GFP intensity of the 20 clones whose depletion reduces the mitochondrial stress response in *sgk-1* mutants. **C.** Length of the worms (µm) upon depletion of the 20 candidates in *sgk-1* mutants. **D.** Quantification of the UPR^{mt} reporter (left upper panel) and worm area (left bottom panel) in wild type animals and *sgk-1* mutants upon depletion of *sbp-1* and *nhr-8* (Mean ± SD; **** p value < 0.0001, *** p value < 0.001, ** p value < 0.005 compared against control(RNAi); *t*-test). Representative images of the expression level of the UPR^{mt} reporter are shown in the right upper panel, brightfield images in the right bottom panel.

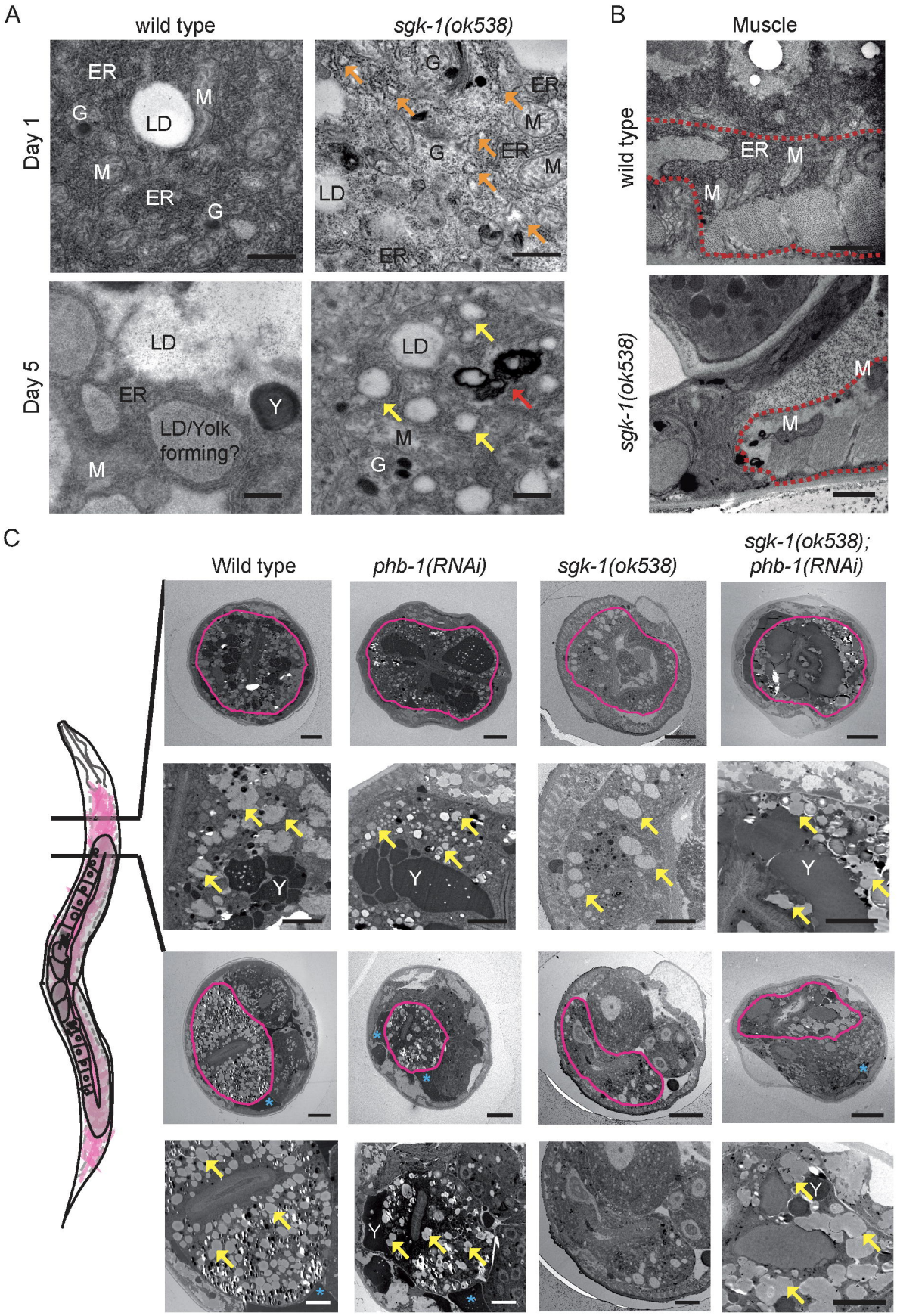

Figure 3: Prohibitin depletion suppresses lipogenesis and lipoprotein/yolk formation defects of *sgk-1* mutants. A. Transmission electron microscopy (TEM) images of the first intestinal cells of wild type and *sgk-1* mutants during aging (day 1 and day 5 of adulthood). Orange arrows point to defective ER exit sites. Yellow arrows point to forming LD. Red arrow, point to abnormal autolysosomes/myelinated forms. Bar size: 500 nm. ER: Endoplasmic Reticulum, LD: Lipid Droplet, Y: Yolk, G: Golgi. **B**. TEM images of muscle, delineated with a red dashed line, of wild type and *sgk-1* mutants at day 1 of adulthood. Bar size: 1 µm. M: Mitochondria **C**. TEM images of wild-type, *sgk-1* mutants, *phb-1* depleted animals and *sgk-1;phb-1(RNAi)* treated mutants at day 5 of adulthood. Two sections, before the gonad and after the gonad turn are shown. Of each section, top images show a general view where the intestine is delineated with a pink line. Bottom images show a magnification of the intestinal area. Bar sizes: 10 µm (top panels) and 5 µm (bottom panels) for each of the cuts. Y: Yolk, blue asterisks mark pseudocoelomic lipoproteins and yellow arrows label LD.

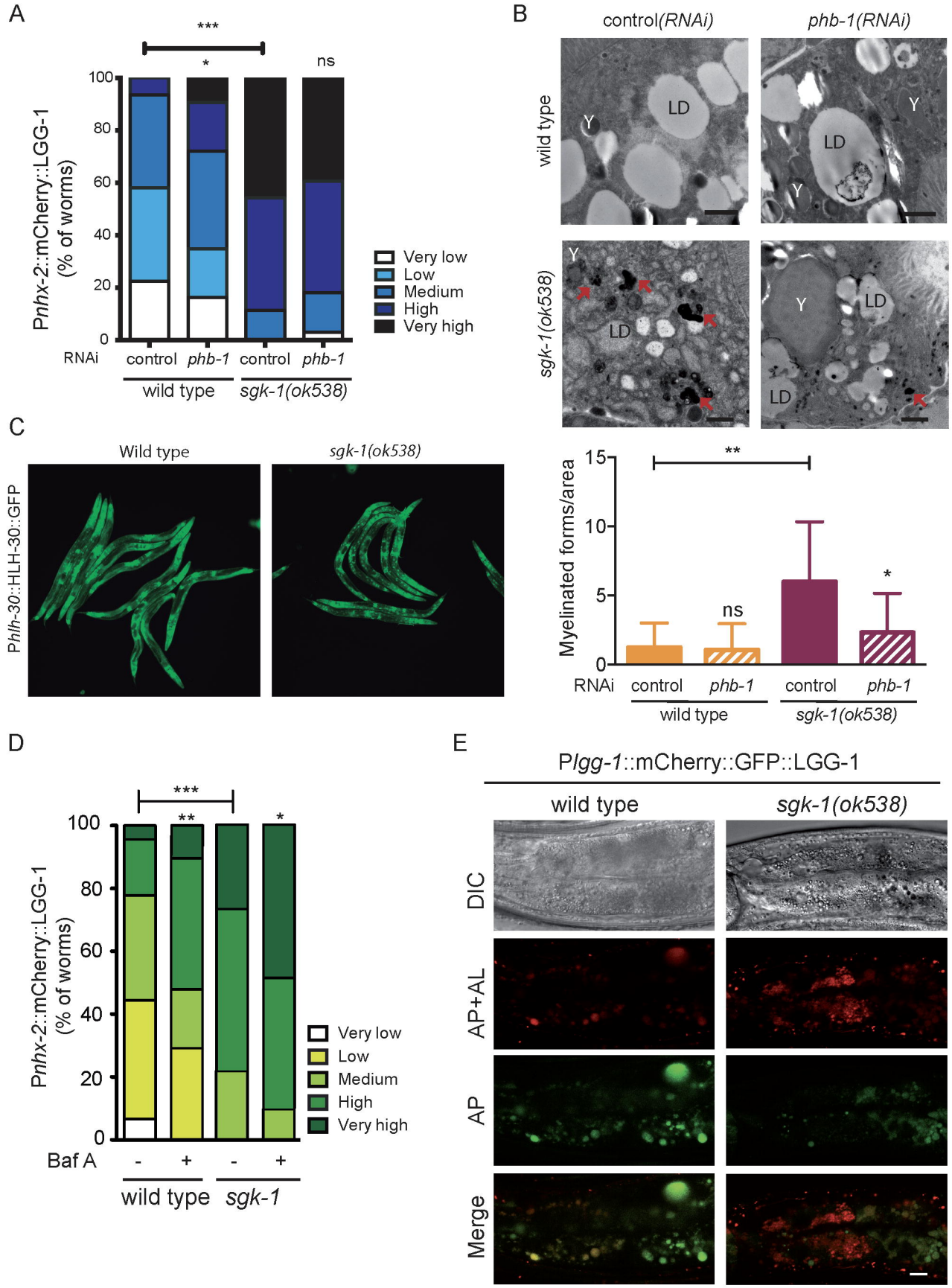

Figure 4: Prohibitin depletion suppresses the impaired autophagy flux of sgk-1 mutants. A. Quantification of the intestinal autophagy reporter Ex[P*nxh-2*::mCherry::LGG-1] (see Fig. S5) in wild type animals, *phb-1* depleted worms, *sgk-1* mutants and *sgk-1;phb-1(RNAi)* treated mutants at day 5 of adulthood. **B.** Electron microscopy images of the same genotypes as in A, at day 5 of adulthood. Red arrows show myelinated forms quantified in the bottom panel. LD: lipid droplet, Y: yolk particles. Bar size: 1µm. **C.** Images of the reporter P*hlh-30*::HLH-30::GFP in wild type and *sgk-1* mutants at day 1 of adulthood in OP50. **D.** Quantification of the intestinal autophagy reporter Ex[P*nxh-2*::mCherry::LGG-1] in wild type animals and *sgk-1* mutants, treated or not with bafilomycin A1 (Baf A), at day 5 of adulthood in HT115. **E.** Images of the reporter P*lgg-1*::mCherry::GFP::LGG-1 in wild type animals and *sgk-1* mutants at day 5 of adulthood in OP50. Brightfield images are shown in the upper panel, red images correspond to autophagosomes (AP) and autolysosomes (AL) and green images correspond only to autophagosomes. Bottom panel show merged images. Bar size: 10 µm. (Mean ± SD; *** p value < 0.001,** p value < 0.01, * p value < 0.1, ns not significant; t-test. Combination of three independent replicates).

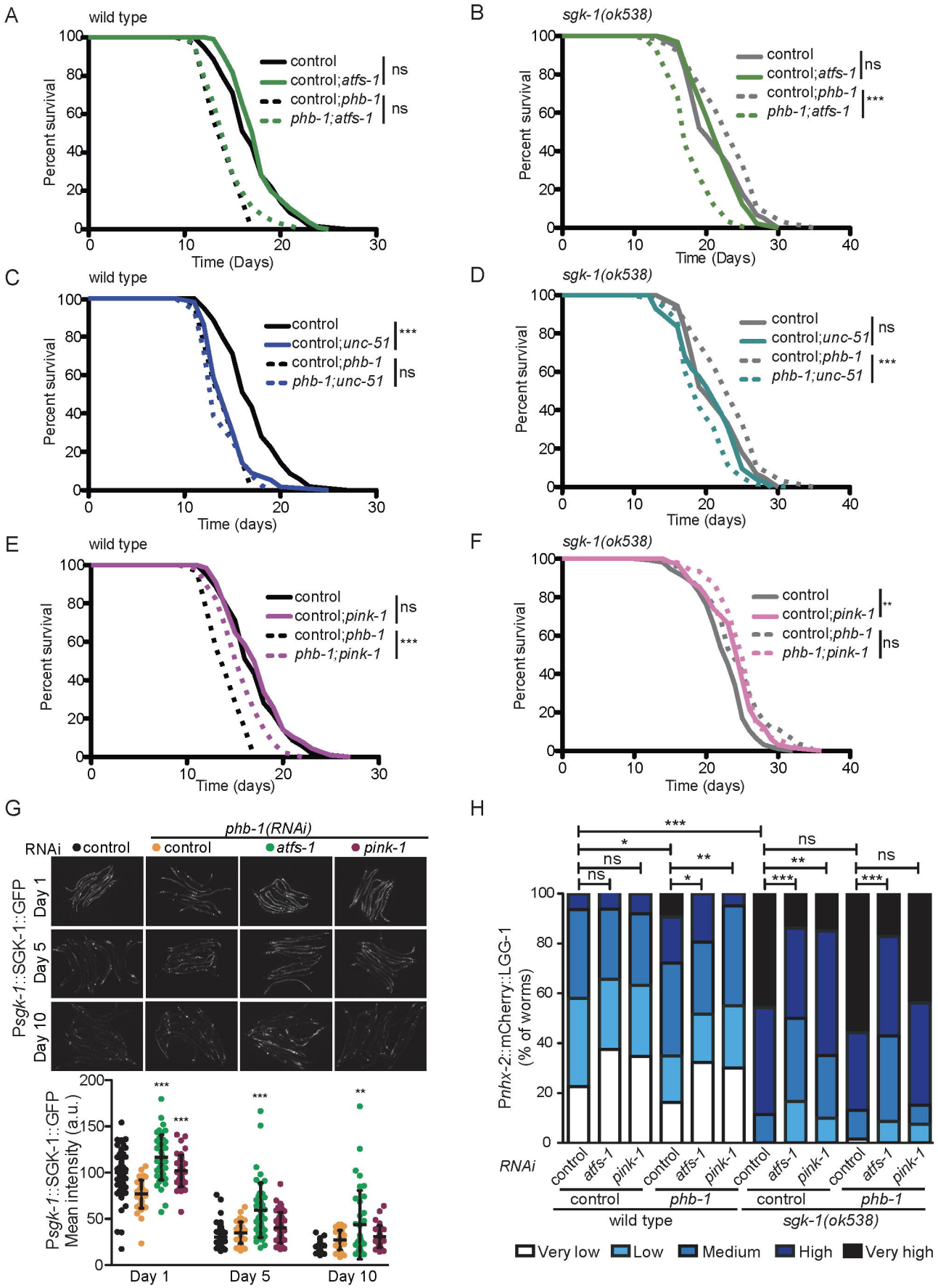

Figure 5: **Autophagy and the UPR^{mt}, but not mitophagy, are required for the enhanced longevity of *sgk-1* mutants upon PHB depletion.** Lifespan of wild type worms (left) and *sgk-1* mutants (right) under normal and mitochondrial stress conditions (*phb-1(RNAi)*) upon inhibition of the UPR^{mt} (**A** and **B**), inhibition of autophagy (**C** and **D**) and inhibition of mitophagy (**E** and **F**). One representative replicate is shown. Replicates and statistics are shown in Table S1. **G**. SGK-1 protein levels at day 1, day 5 and day 10 of adulthood measured using the Psgk-1::SGK-1::GFP reporter, upon PHB depletion and inhibition of either the UPR^{mt} (*atfs-1(RNAi)*) or mitophagy (*pink-1(RNAi)*) (Mean SD; *** p value < 0.001, ** p value < 0.01, * p value < 0.1, ns not significant; ANOVA test. Combination of at least three independent replicates is shown). **H**. Quantification of the autophagy reporter Ex[P*nxh-2*::mCherry::LGG-1] in wild type animals, *phb-1(RNAi)* treated worms, *sgk-1* mutants and *sgk-1;phb-1* depleted mutants at day 5 of adulthood upon inhibition of the UPR^{mt} (*atfs-1(RNAi)*) or mitophagy (*pink-1(RNAi)*) (*** p value < 0.001, ** p value < 0.01, * p value < 0.1, ns not significant; t-test. Combination of at least three independent replicatesis shown).